An investigation of the Dynamics of Phase Transitions in Lennard-Jones Fluids

by

Nicolas Hadjiconstantinou

B.A., Engineering, Cambridge University, U.K. (1993)
S.M., Mechanical Engineering, Massachusetts Institute of Technology (1995)
M.A., Engineering, Cambridge University, U.K. (1997)

Submitted to the Department of Physics
in partial fulfillment of the requirements for the degree of

Master of Science in Physics

at the

MASSACHUSETTS INSTITUTE OF TECHNOLOGY

August 1998

Author .....
Department of Physics
July 15, 1998

Certified by .....
Tomás A. Arias
Assistant Professor
Thesis Supervisor

Accepted by .....
Thomas J. Greytak
Associate Department Head for Education

An investigation of the Dynamics of Phase Transitions in Lennard-Jones Fluids

by

Nicolas Hadjiconstantinou

Submitted to the Department of Physics
on July 15, 1998, in partial fulfillment of the
requirements for the degree of
Master of Science in Physics

Abstract

This thesis reports the development, validation and application of a method to simulate external heat addition in molecular dynamics simulations of Lennard-Jones fluids. This simulation capability is very important for both purely theoretical and practical applications. Here we examine one theoretical application, namely the evaporation of clusters of liquid Argon under constant pressure.

The algorithm is based on modified equations of motion derived from Newton's equations with the use of what is known in the literature as Gauss' least constraint principle. The modified equations of motion satisfy the constraint of linear (in time) energy addition to all the system molecules.

The first part of the thesis presents the validation of the heat addition algorithm: the method is useful only if it does not adversely affect the properties of the simulated material. The validation consists of a series of simulations of a Lennard-Jones fluid in a two–dimensional channel bounded between two parallel (molecular) walls. The walls are kept at constant temperature, while the fluid is externally heated using the new simulation method. The temperature profile solution for this problem is, according to (the exact) continuum theory, parabolic. Given the heat addition rate, estimates for the value of the thermal conductivity can be obtained from the curvature of the temperature profile. The estimates for the thermal conductivity are compared to experimental data for the fluid, and simulation data based on the Newtonian (exact) equations of motion for the same fluid. We find that the thermal conductivity estimates obtained from our simulations are in agreement with the baseline results utilizing the Newtonian equations of motion.

The second part of the thesis reports on the investigation of the phase change of fluid clusters at constant pressure in real time using the heat addition algorithm. This has not been attempted before; results exist in the literature only for quasistatic simulations whereby the phase change behavior of a Lennard-Jones fluid is recovered by performing a series of equilibrium simulations at varying temperatures. The results obtained through the newly proposed, developed, and validated time dependent method are in agreeement with the results of the quasistatic simulations as linear

response theory predicts.

We conclude with the interpretation of our results using homogeneous nucleation theory. We find that our results are consistent with homogeneous nucleation which predicts that phase separation starts at the nanoscopic level with critical radii of the order of a few nanometers for both evaporation and condensation. The critical nuclei for evaporation, which are gaseous, are predictably larger than the nuclei for condensation, which are in the liquid state. Our results are in good agreement with experimental data.

This work can form the basis for the investigation of open problems related to nucleation theory and nucleation kinetics, such as metastable cluster lifetimes, and nucleation frequencies. Alternative phase change mechanisms, such as spinodal decomposition, can also be investigated.

Thesis Supervisor: Tomás A. Arias
Title: Assistant Professor

Acknowledgments

I would like to thank my thesis advisor Professor Tomás A. Arias for his very helpful comments and help during the preparation of this thesis. His willingness to supervise and contribute to this thesis is greatly appreciated.

My warmest thanks to Professor Nihat Berker for his continuous support, encouragement, and help during the course of this work but also for introducing me to the world of statistical mechanics.

I am grateful to the other members of my research group, Marius Paraschiviou, Miltos Kambourides, Jeremy Teichman, Serhat Yesilyurt, John Otto, and Luc Machiels. They have provided me with technical advice, intellectual stimuli but also invaluable friendship.

My friends at MIT, Ilias Argiriou, Miltos Kambourides, Panayiotis Makrides, Alexandros Moukas, Natasa Stagianou, and Elias Vyzas have made these five years not only possible but also enjoyable. I will always cherish their love, understanding, and encouragement. Special thanks to my "family in Boston", Dr. Wolf Bauer, Antonis Eleftheriou, Chris Hadjicostis, Maria Kartalou, Karolos Livadas, Panayiota Pyla, Ozlem Uzuner, Andreas Savvides, and George Zacharia. I have been privileged to be a member of the Kb group and a great admirer of the founder and leader Andreas Argiriou.

Special thanks to my parents Athena and George, and my sister Stavroulla for their love and encourangement.

I am indebted to Dr. Keith Refson for the developement of the molecular dynamics simulation code MOLDY.

Στους γονείς μου

Αθηνά και Γιώργο,

και στην αδελφή μου

Σταυρούλλα

Contents

List of Figures

List of Tables

Chapter 1

Introduction

Thermodynamics and statistical mechanics have been very successful in explaining and predicting the behavior of many physical systems. While thermodynamics describes systems in equilibrium, the notion of local equilibrium has allowed the extension of thermodynamic results to non-equilibrium, steady-state situations. Time varying situations can also be reduced, according to linear response theory [10], to a series of quasiequilibrium states; systems respond (in time) to external fields by utilizing fluctuations around their equilibrium states to move to a neighboring equilibrium state.

Computer simulations of phase change of small statistical mechanical systems, such as constant pressure evaporation of a Lennard-Jones fluid, have been limited, to the author's knowledge, to series of quasistatic simulations [4, 12, 21, 23], primarily using Monte Carlo (MC), or Molecular Dynamics (MD) techniques. We use the term "series of quasistatic simulations" to denote series of equilibrium numerical experiments used to map the phase diagram of a fluid. These simulations report hysteritic effects [4, 12, 2] and the existence of metastable equilibrium states which resemble the van der Waals equation of state behavior in the two phase region (see Fig 1-1). This behavior has traditionally been considered [4, 13] to be an artifact of the small number of particles in the system, which is insufficient to sample a rich enough phase space, and consequently unable to reproduce the most probable sequence of macrostates which would be observed in the thermodynamic limit ($V \to \infty, N \to$

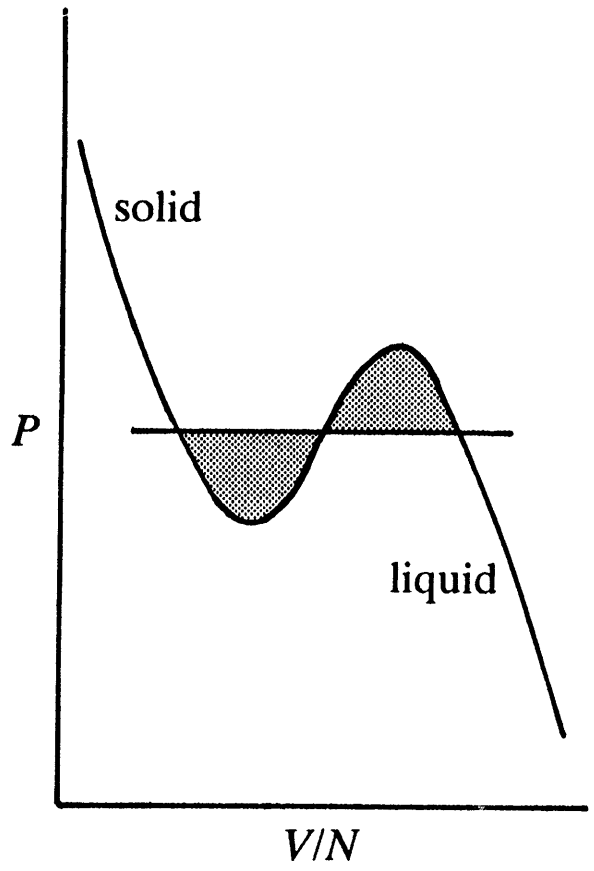

Figure 1-1: Sketch of hysteritic behavior in a P-V diagram (from [4]). The indicated areas are equal.

$\infty, V/N = const.$), namely that the constant pressure evaporation of a fluid takes place at constant temperature.

We have developed a method to simulate heat addition in an MD simulation in order to study the evaporation of a Lennard-Jones fluid in real time in an attempt to elucidate the above issues and observations and obtain a better understanding of phase change as a time dependent phenomenon in general. This method utilizes Gauss' principle of least constraint to derive equations of motion that simulate constant (in time) heat addition to the simulated particles. This principle has been widely used in the literature to derive equations of motion that simulate systems at constant temperature, known as the "thermostated equations of motion".

In particular, we first want to verify that our time dependent simulations would display the same behavior as that observed in quasistatic simulations. According to

linear response theory [10], time dependent simulations should "smoothly join" the discrete points yielded by quasistatic simulations. Second, we want to demonstrate that metastable states, which are indeed negligible in the thermodynamic limit [13], are inherent in any realistic description of phase change. In other words, the thermodynamic limit is not necessarily relevant in real world experiments or indeed MD simulations.

Homogeneous nucleation theory states that evaporation (condensation) is initiated by small clusters of fluid which due to spontaneous fluctuations have a small but finite probability to be in the gaseous (liquid) state at some instant in time. If the conditions are favorable, this small vapor bubble (liquid drop) will grow and proceed to convert more liquid to vapor (vapor to liquid). The conditions under which these nuclei can exist are determined by the free energy involved in their formation. Once the nuclei attain a certain critical size they can grow. The size of these nuclei is finite and therefore the supersaturated fluid is said to be in a metastable state. This critical size becomes monotonically smaller with increasing supersaturation. The rate at which nuclei are spontaneously formed is the other determining factor for the critical supersaturation required: it is an exponentially decreasing function of their size. The rate of spontaneous generation of nuclei is the subject of nucleation kinetics which we will not examine here. In conclusion, phase transition will proceed when the supersaturation is such that the rate of generation, or probability of existence, of critical, or larger, nuclei has reached a finite value that is expected to be material dependent.

As the supersaturation is increased and the spinodal (locus of extrema of an isobar (constant pressure) in a T-S diagram) is approached, the above critical nuclei become vanishingly small. Upon reaching the spinodal the fluid becomes unstable to all perturbations exceeding a critical wavelength [7], and the fluid changes phase by the process of spinodal decomposition. Spinodal decomposition is best known in alloy solidification processes where rapid quenches are used to exploit the effects of spinodal decomposition on the material microstructure and the resulting mechanical properties. The seamless transition from homogeneous nucleation to spinodal

decomposition is the subject of current research [7].

The importance of metastable states has been recognized very long ago [9], but experimental verification has had limited success to date [27]. It is well known that metastable states are difficult to reproduce experimentally because of impurities and finite size nucleation sites available in real systems. Molecular dynamics, however, is inherently free of such disturbances and would be expected to complement the most careful real world experiments nicely. It also provides a unique opportunity to study this transition from homogeneous nucleation to spinodal decomposition under "controlled experimental conditions".

Chapter 2

Molecular Dynamics

Despite the molecular nature of matter, for most hydrodynamic applications of interest, the continuum description of nature successfully captures all the essential physics while resulting in a significantly more tractable formulation. There exist, however, situations where the continuum description is inadequate; such situations are described in the following chapters. In this case we need to resort to the molecular description and use the classical tools of statistical mechanics. Unfortunately statistical mechanics has traditionally been limited by the intractability and complexity of the governing equations describing the systems of interest. For fluids, the BBGKY hierarchy of equations [14] has been tackled for very few special cases, dilute gases being the most notable. The advent of fast and powerful computers has brought a revolution to the molecular modelling of nature; numerical solutions of the BBGKY equations can be obtained for more complicated cases, but more importantly, systems can be *animated* at the molecular level through molecular dynamics (MD).

In the molecular dynamics presented in this thesis, systems are modelled as collections of molecules that obey a set equations of motion (classical Newtonian) and interact among themselves through intermolecular interaction potentials. MD is a very powerful technique because, as long as the interaction potentials are specified for the systems under investigation, no approximations or further modelling is required; all the exact physics is present and accounted. The major disadvantage is the high computational cost associated with these computations which limits the use of

this technique to very small systems and very short timescales (of the order of ten thousand molecules and $1ns$ in time for a high-end workstation).

2.1 Preliminaries

Although in the most general formulation of statistical mechanics particles interact through quantum mechanical equations of motion, it is often the case that many systems can be simulated to a sufficient approximation by the use of the classical Newtonian equations of motion

$$\ddot{\vec{r}}_i = -\frac{1}{m_i}\sum_{j\neq i}\frac{1}{r_{ij}}\frac{dV(\vec{r}_{ij})}{dr_{ij}}\vec{r}_{ij}\ , \tag{2.1}$$

where m_i is the mass of the particle, $\vec{r}_i$ is the position vector of the particle with respect to the coordinate origin, $\vec{r}_{ij} = \vec{r}_i - \vec{r}_j$, $V(\vec{r}_{ij})$ is the potential energy of particle i due to particle j and the sum is implied to be over all particles (N). This simplification, which results in significantly less computationally intensive calculations, will in general be valid when all quantum mechanical effects (both temporal and spatial) are negligible, or can be reliably lumped in an effective interaction potential $V(\vec{r}_{ij})$ and the effects of zero point motion can be ignored. This is almost always the case for the hydrodynamic applications presented in this thesis, and as a result we will limit ourselves to the exclusive use of the classical equations of motion.

The interaction potential used in this study is the well known [4] Lennard-Jones potential

$$V(\vec{r}_{ij}) = 4\varepsilon[(\sigma/r_{ij})^{12} - (\sigma/r_{ij})^{6}]. \tag{2.2}$$

This simple model was chosen for its ability to minimize the computational cost of calculations while retaining all the essential physics under investigation. The Lennard-Jones potential has been shown [4] to accurately reproduce the properties of noble gases with appropriate choice of the two parameters ε and σ. The Lennard-Jones potential can also be used in studies of water [11] (in conjunction with an electrostatic potential), and light hydrocarbons. It provides a reasonable compromise between nu-

merical efficiency and accuracy for hydrodynamic applications where a "hard sphere" approximation often suffices. Structural or thermodynamic properties of materials other than noble gases are not reproduced accurately. The great computational efficiency enjoyed form the use of this potential is a result of two effects: first, the potential has a short range and effectively decays to zero for $r > 10\sigma$ thus leading naturally to the definition of an interaction sphere that contains all the particles contributing to the force acting on a specific particle, and second, it is a pairwise additive potential and hence the force acting on a simulated particle can be simply calculated by adding the forces exerted to it by the other particles that are within its interaction sphere. Because the number of molecules within a sphere of radius r increases as $n \propto r^3$, researchers have attempted to use interaction spheres (defined by the interaction cut-off r_c) smaller than 10σ. It has been shown [30] that the error resulting form the use of cut-offs as small as 2.2σ is negligible. Throughout this study we have used a conservative value of $r_c = 3\sigma$.

The equations of motion are numerically integrated using Beeman's modified equations of motion [26], which is a fourth order accurate in space and third order accurate in time predictor corrector method. It is included here for completeness: if x is any dynamic variable (in our case $\vec{r}_{ij}$), $\dot{x}^{(p)}, \dot{x}^{(c)}$ are the predicted and corrected corresponding velocities, and Δt is the numerical integration timestep, the scheme is as follows

1. $x(t+\Delta t) = x(t) + \Delta t\dot{x}(t) + \frac{\Delta t^2}{6}[4\ddot{x}(t) - \ddot{x}(t-\Delta t)]$
2. $\dot{x}^{(p)}(t+\Delta t) = \dot{x}(t) + \frac{\Delta t}{2}[3\ddot{x}(t) - \ddot{x}(t-\Delta t)]$
3. $\ddot{x}(t+\Delta t) = F(x_i(t+\Delta t), \dot{x}_i^{(p)}(t+\Delta t), i = 1...N)/m$
4. $\dot{x}^{(c)}(t+\Delta t) = \dot{x}(t) + \frac{\Delta t}{6}[2\ddot{x}(t+\delta t) + 5\ddot{x}(t) - \ddot{x}(t-\Delta t)]$
5. Replace $\dot{x}^{(p)}$ with $\dot{x}^{(c)}$ and goto 3. Iterate to convergence.
6. Update t from $t+\delta t$. Go to 1.

Here F is the total force acting on a particle and N is the total number of particles in the simulation.

The simulation procedure discribed above produces realizations of the microcanonical ensemble, which in many cases are not good approximations to the system under investigation. In particular, it is sometimes useful to let the volume of the system vary and constrain the pressure of the system at an imposed pressure P thus realizing a constant pressure ensemble. In what follows we review the reformulation of the equations of motion pioneered by Parinello and Rahman [22] which allows the simulation of a system under constant pressure situations.

2.2 Constant Pressure Simulations

In the formulation of Parinello and Rahman [22, 26] the molecular dynamics simulation cell is allowed to change in size in response to the imbalance between the imposed pressure and the internal simulation pressure. The new equations of motion are written in the center of mass co-ordinates ($\vec{s}_i$)

$$m_i \ddot{\vec{s}}_i = \mathbf{h}^{-1} \nabla \sum_{j \neq i} V(\vec{r}_{ij}) - m_i \mathbf{G}^{-1} \dot{\mathbf{G}} \dot{\vec{s}}_i. \tag{2.3}$$

Here $\vec{s}_i = \mathbf{h}^{-1}\vec{r}_i$, $\mathbf{h}$ is the 3×3 matrix whose columns are the molecular dynamics cell vectors, and $\mathbf{G} = \mathbf{h}^T\mathbf{h}$. Additionally the cell vectors obey the following dynamical equation

$$W\ddot{\mathbf{h}} = (\mathbf{T} - \mathbf{p})\mathbf{k} \tag{2.4}$$

where W is the fictitious mass parameter of the pressure reservoir in equilibrium with the system, $\mathbf{k} = V\mathbf{h}^{T^{-1}}$, V is the volume of the system, $\mathbf{p}$ is the external stress (tensor) applied to the system, and $\mathbf{T}$ is the molecular contribution to the stress tensor defined by

$$\mathbf{T} = \frac{1}{V}\left(\sum_i^N m_i \dot{\vec{r}}_i \dot{\vec{r}}_i - \sum_i^N \sum_{j>i}^N \frac{1}{r_{ij}} \frac{dV(\vec{r}_{ij})}{dr_{ij}} \vec{r}_{ij} \vec{r}_{ij}\right). \tag{2.5}$$

Note that the above definition (eq. (2.5)) assumes that the system has a uniform pressure throughout and hence it is in pressure equilibrium. The definition and evaluation

of thermodynamic properties as a function of space in nonequilibrium situations is obtained via the use of the assumption of local thermodynamic equilibrium discussed in section 2.5.

2.3 Simulation Reduced Units

It is also customary to define reduced units based on the molecular model of the material simulated [4]. In both series of simulations reported in this work the principal material used was fluid Argon and hence unless otherwise stated, all quantities will be expressed in reduced units using $\sigma = 3.4$ Å for length, $m = 40$ amu for mass, $\varepsilon/k_b = 119.8^o K$ for temperature, and $\tau = (m\sigma^2/48\varepsilon)^{1/2} = 3.112 \times 10^{-13} s$ for time. Here σ and ε are the parameters of the Lennard-Jones (LJ) potential for Argon [4], m is the mass of the Argon atom, and τ is the characteristic time for Argon. The integration timestep was $\Delta t = 0.032\tau$. The characteristic length σ is the characteristic (hard sphere) size of a molecule; the potential well minimum is at $r = 2^{1/6}\sigma$. The characteristic time τ corresponds to the inverse natural frequency of oscillation of an Argon dimer.

It is sometimes customary to denote reduced quantities with the starred symbol of their non-reduced counterparts. We do not adopt this convention but we note that some figures we have taken from references [16, 24, 31] make use of this convention.

2.4 The Heat Addition Model

2.4.1 Gauss' Principle of Least Constraint

We briefly summarize Gauss' principle of least constraint [8] which is part of Gauss' formulation of a mechanics more general than Newton's. In this mechanics, Newton's equations of motion follow as a special case in which no constraints are imposed on the system under investigation. For systems subject to a constraint G, the equations

are found by minimizing the square of the curvature

$$C = \frac{1}{2}\sum_i m_i(\ddot{\vec{r}}_i - \frac{\vec{F}_i}{m_i})^2 \tag{2.6}$$

subject to that constraint. Here $\vec{F}_i$ is the force acting on molecule i, and C is a function of the set of accelerations $\ddot{\vec{r}}_i$. This procedure guarantees that the phase space trajectories followed, deviate minimally from the Newtonian trajectories in the least-squares sense [8]. For holonomic constraints this principle and the least action principle yield exactly the same results. For nonholonomic constraints, however, Gauss' principle does not follow from a Hamiltonian and it is not equivalent to the least action principle [8].

The minimization can be achieved by using the method of Lagrange multipliers: the curvature C is a function of accelerations only, and hence we obtain the constrained equations of motion by solving

$$\frac{\partial}{\partial \ddot{\vec{r}}_i}(C - \lambda G) = 0, \tag{2.7}$$

given that we have expressed the constraint G as a function of the accelerations $\ddot{\vec{r}}_i$. If we set $G = 0$ in eq. (2.7), we recover the Newtonian equations of motion (eq. (2.1)).

2.4.2 Heat Addition Equations of Motion

In this section we use Gauss' principle of least constraint to derive equations of motion that simulate a constant (in time) heat addition per unit particle (modeling for example internal heat generation due to the passage of electrical current through an electrolyte). The equations of motion for the heat addition are obtained by incorporating the following constraint

$$\frac{1}{2}\sum_i \left(m_i \dot{\vec{r}}_i^{\,2} + \sum_{j \neq i} V(\vec{r}_{ij}) \right) = E_o + N\dot{Q}t, \tag{2.8}$$

in the Newtonian equations of motion, in the Gaussian least constraint sense explained above. Here $\dot{Q}$ is the rate of energy addition per particle and E_o is the initial energy (of all particles). The constraint requires that the total energy of the simulation rises linearly in time. Differentiating once with respect to time the constraint equation (2.8) we obtain

$$G(\ddot{\vec{r}}_i) = \sum_i \left(m_i \dot{\vec{r}}_i \ddot{\vec{r}}_i - \frac{1}{2} \vec{F}_i \cdot \dot{\vec{r}}_i - \frac{1}{2} \sum_j \vec{F}_{ji} \cdot \dot{\vec{r}}_j \right) - N\dot{Q} = 0. \tag{2.9}$$

To obtain the constrained equations of motion, we solve

$$\frac{\partial}{\partial \ddot{\vec{r}}_i} \left(\frac{1}{2} \sum_j m_j (\ddot{\vec{r}}_j - \frac{\vec{F}_j}{m_j})^2 - \lambda \left(\sum_i (m_i \dot{\vec{r}}_i \ddot{\vec{r}}_i - \vec{F}_i \cdot \dot{\vec{r}}_i) - N\dot{Q} \right) \right) = 0, \tag{2.10}$$

to obtain

$$\ddot{\vec{r}}_i = -\frac{1}{m_i} \nabla \sum_{j \neq i} V(\vec{r}_{ij}) - \lambda(\dot{\vec{r}}_i) \dot{\vec{r}}_i \tag{2.11}$$

with

$$\lambda(\dot{\vec{r}}_i) = -\frac{N\dot{Q}}{\sum_i^N m_i \dot{\vec{r}}_i{}^2}. \tag{2.12}$$

In obtaining equation (2.10) we used the fact that equation (2.9) can be written as

$$G(\ddot{\vec{r}}_i) = \sum_i \left(m_i \dot{\vec{r}}_i \ddot{\vec{r}}_i - \vec{F}_i \cdot \dot{\vec{r}}_i \right) - N\dot{Q} = 0, \tag{2.13}$$

which follows from

$$\sum_i \sum_j \vec{F}_{ji} \cdot \dot{\vec{r}}_j = \sum_j \vec{F}_j \cdot \dot{\vec{r}}_j = \sum_i \vec{F}_i \cdot \dot{\vec{r}}_i. \tag{2.14}$$

To obtain equation (2.12) we have substituted equation (2.11) in equation (2.9), or equivalently, equation (2.13).

It can easily be shown [5] that in the case of small heat addition the above equa-

tions can be linearized to the following rescaling algorithm,

$$\ddot{\vec{r}}_i = -\frac{1}{m_i}\nabla \sum_{j \neq i} V(\vec{r}_{ij}) \tag{2.15}$$

and

$$\dot{\vec{r}}_i = -(\lambda(\dot{\vec{r}}_i) + 1)\Delta t\, \ddot{\vec{r}}_i, \tag{2.16}$$

which is similar to the rescaling algorithm widely used to remove heat (although in a constant temperature formulation) from simulations. This formulation will be useful since, as discussed later, it has better numerical solution characteristics than the original formulation (equations (2.11) and (2.12)).

It has been shown [8] that the equations resulting from the application of Gauss' principle of least constraint to the case of a constant temperature simulation, indeed reproduce the correct (canonical ensemble) dynamics in the constant temperature (equilibrium) case. Care, however, has to be taken in nonequilibrium situations since there has been no extension of the above result in the latter case. We expect that, since both sets of equations (2.11) and (2.12), or (2.15) and (2.16), reduce to the Newtonian equations of motion for $\lambda \to 0$, the model dynamics will not be significantly different than the "correct" nonequilibrium dynamics for small λ.

We remark that our model interprets heat addition as an acceleration in the direction of the velocity $\dot{\vec{r}}_i$ of the molecule. Despite the slightly artificial nature of this interpretation, we believe that if the heat addition rate is small enough, or equivalently, the heat addition timescale is long enough compared to the collision timescale (τ), then complete thermalization of the added energy will occur sufficiently fast for the system to be in the "correct" nonequilibrium state at every instant in time. This assumption is very important for the calculation of entropy S as we also remark later. An estimate for the heat addition timescale is given by $\tau_Q = E/\dot{Q}$. In our simulations $\tau_Q \sim 1000\tau \gg \tau$; we thus expect that the assumption of complete thermalization is valid.

2.5 Definition of Macroscopic Properties

From a statistical mechanical point of view molecular dynamics numerically simulates the motion of the system under consideration in a $6N-$dimensional phase space. As a result, MD simulation results are in the form of position coordinates and velocities of the N system molecules for a large number of timesteps (duration of the simulation). In order to convert those to the usual macroscopic thermo-hydrodynamic parameters we need to establish a "macroscopic connection". In statistical mechanics this is done through the use of ensembles: observables (parameters that are macroscopically perceived, such as energy, temperature, pressure, and desity) are defined as functions of the molecular information and evaluated at every timestep. Due to the huge number of degrees of freedom of the molecular system, it is conceivable that a huge number of molecular configurations will lead to the same values of observables leading to what is usually called "loss of information". On the other hand these macroscopic observables will fluctuate as the particles continuously change positions and momenta. The "macroscopic connection" is made through the use of an ensemble of identical systems such that the macroscopic quantity or parameter is defined as the average of the observable over all the ensemble members. In the following section we describe the extension of the equilibrium ideas to the local thermodynamic equilibrium formulation that allows the treatment of nonequilibrium situations.

2.5.1 Local Thermodynamic Equilibrium

The concept of local thermodynamic equilibrium allows the extension of thermodynamic equilibrium techniques to spatially nonequilibrium systems. It is the equivalent of the quasistatic assumption for time-varying systems, and essentially assumes that although the system is not in equilibrium it can, to a good approximation, be assumed to be in equilibrium locally in space (versus time for the quasistatic case). This assumption can be reasonable if the gradients in the system are sufficiently small. In particular, we require that the change across a region (spatial case) due to the nonequilibrium gradients present, be smaller than the statistical fluctuations

in this region because of its small size. For the temporal case we require that the rate of change due to some external driving field is much smaller compared to the characteristic equilibration frequency of the fluid, $1/\tau$.

For the spatial case, this essentially implies that the larger the gradients, and hence the larger the deviation from equilibrium, the smaller these regions need to be. Trozzi et al. [34] have verified that this concept can be used to define *local* macroscopic properties in MD simulations. For the gradients present in their work, they found that regions of characteristic size σ (containing $O(10)$ molecules) can, to a good approximation, be assumed to be in local thermodynamic equilibrium. We will be using the same criterion since the gradients present in our work are very similar to the work of Trozzi et al.

In fact, we can show that in order to simulate the smallest gradients possible (in an attempt to make the simulation as realistic as possible) we need to increase the number of molecules by adding the extra molecules in the direction of the gradient. The fluctuations $\Delta\chi_F$ of a property χ in a region of space Ω containing N molecules scale as $\Delta\chi_F \propto 1/\sqrt{N}$. The variation of the above property $\Delta\chi_g$ along the direction of the gradient g is given by $\Delta\chi_g = gL$ where L is the linear dimension of Ω in the direction of g. We require that $\Delta\chi_g \sim \Delta\chi_F$ and hence,

$$gN^d \propto N^{-1/2}. \tag{2.17}$$

We have substituted L with N^d where d takes different values depending on the "mode" of addition of molecules. If molecules are added equally in all dimensions $d = 1/3$; if the molecules are added in the direction of the gradient g, $d = 1$; finally, if the molecules are added in the remaining directions only, $d = 0$. It follows that the optimum scaling (least number of molecules for a given gradient) obtains for the case of molecule addition in the direction of the gradient for which

$$N \propto g^{-2/3}. \tag{2.18}$$

As an example, consider the case of a fluid in a two-dimensional channel with the

two bounding walls at different temperatures. For a given number of molecules and fixed wall temperatures (or temperature difference), the minimum gradient that can be simulated is obtained by maximizing the number of molecules in the transverse channel direction, the direction normal to the two walls.

We would like to note that the smaller the local equilibrium regions the smaller the number of particles that reside in it. Hence, although in theory an arbitrarily small region can always be found that can be assumed to be in local equilibrium, this is not practical for regions much smaller than the ones used in this study because of the unreliable statistics obtained from these very small domains due to the very small number of molecules in them, since as discussed above the directions transverse to the gradient do not typically contain an appreciable number of molecules. Additionally, regions smaller than the characteristic size σ are not admissible on physical grounds since this length scale sets the lower limit for the spatial region over which the concept of a fluid exists.

2.5.2 Statistical Mechanical Properties

In this section we present the definitions of macroscopic observables such as temperature and pressure in terms of microscopic properties. These definitions, are the first step in the macroscopic connection required to recover a spatially varying thermo-hydrodynamic field over the MD simulation domain from the molecular data. The following definitions can be obtained through statistical mechanical analysis [15]; in particular, the macroscopic conservation laws are obtained through an ensemble averaging of the corresponding microscopic conservation laws. The identification of single particle contributions to the macroscopic observables follows from the direct comparison of the microscopic ensemble averaged equation and its continuum counterpart. For the derivation of these relations the reader is referred to the original work of Kirkwood and Buff [15].

Let V be the volume in which we want to define the macroscopic observable A_V.

Following [29, 34] we define

$$A_V = \frac{1}{V}\int_V d\vec{r}\sum_{i=1}^{N} A_i \delta(\vec{r} - \vec{r}_i) \tag{2.19}$$

where N is the number of molecules, and $A_i = A_i(\{\vec{r}_j, \vec{p}_j\}_{j=1,N})$ is the individual particle (i) contribution to the macroscopic property A_V. Again following [34], we define for the density (ρ_V)

$$A_i = 1, \tag{2.20}$$

for the temperature (T_V)

$$A_i = \frac{m_i \dot{r}_i^2}{3k_B \rho_V} \tag{2.21}$$

where k_B is Boltzmann's constant, for the internal energy (E_V)

$$A_i = \frac{\sum_{j \neq i} V(\vec{r}_{ij})}{2\rho_V}, \tag{2.22}$$

for the flow velocity ($\vec{v}_V$)

$$A_i = \dot{\vec{r}}_i, \tag{2.23}$$

and for the stress tensor (Π_V)

$$A_i = m_i(\dot{\vec{r}}_i - \vec{v}_V)(\dot{\vec{r}}_i - \vec{v}_V) - \frac{1}{2}\sum_{j \neq i} \vec{r}_{ij} \frac{1}{r_{ij}} \frac{dV(\vec{r}_{ij})}{dr_{ij}} \vec{r}_{ij}, \tag{2.24}$$

from which the pressure can be evaluated as the trace of the stress tensor ($P_V = \frac{1}{3} Tr(\Pi_V)$). Using the definitions given in the previous section, macroscopic observables can be evaluated over small regions at one instant in time for every member of the ensemble under consideration. Any thermodynamic parameter is then obtained from the ensemble average of this observable over all the members of the ensemble.

2.5.3 Error Estimation

Due to the small number of particles that are available in each local equilibrium domain (bin) the statistical uncertainty associated with the property estimates is

large. Under the assumption of Gaussian statistics the statistical error scales inversely proportional to the square root of the number of samples taken. In our macroscopic world, local equilibrium regions contain more than 10^{20} molecules and as a result the fluctuations within them are imperceptible. In molecular simulations, however, the size of a local thermodynamic equilibrium region, dictated by the the balance of the fluctuations and the magnitude of the gradients in the simulation (eq. (2.6)), is of the order of a few σ. The fluctuations in the value of a quantity ($\delta\chi_F$) in such a domain are often of the order of the value of the quantity itself (χ) and hence the gradients that can actually be resolved involve variations of $O(\chi)$ over distances of a few σ length-scales. Large gradients, however, require smaller local equilibrium regions which contain less molecules and, hence, exhibit larger fluctuations. Simulation accuracy and resolution of physically realistic gradients are thus coupled.

Steady simulations, or simulations that are unsteady on a macroscopic timescale which is long enough such that the problem appears to be steady at the microscale, benefit in terms of accuracy from the use of the ergodic theorem [4] in the exchange of time with ensemble realizations. More precisely, an ergodic system in a steady state left to evolve in time, produces realizations that are equivalent to those obtained by different members of the emsemble used in the formal definition of a statistical mechanical system. Hence the ensemble averaging procedure is replaced by averaging in time which is very convenient for a molecular dynamics simulation which is inherently an integration procedure in time. The system under investigation is thus simulated for an equilibration time that allows for initial condition effects to decay and hydrodynamic transient effects to disappear, and its subsequent configurations are sampled in regular time intervals (of the order of a few integration timesteps).

The expected error in the estimation of a parameter depends on the number of independent samples taken. We could maximize the number of samples taken by sampling every integration timestep. Unfortunately, as discussed above, for reasons of numerical accuracy the integration timestep is a very small fraction (0.032) of the characteristic timescale for the fluid (τ), and hence samples that are temporally less than τ apart are statistically corelated: even if they are used in the sampling proce-

dure they do not contribute any new information and do not reduce the statistical error. Based on physical grounds, we would expect that an appropriate decorelation timescale would be τ. Numerical experiments [4] show that different parameters have different decorrelation timescales, but this physical reasoning is approximately correct. In particular, velocity which is a first moment of molecular velocities, requires $2\tau - 3\tau$, whereas heat flux which is a higher moment but also involves the interatomic forces, requires less than τ.

Chapter 3

Model Validation

In the previous chapter we showed that equations of motion can be written to simulate uniform heat addition (in space). Before applying this technique to the evaporation problem we would first like to validate that it has no adverse effects on the macroscopic properties of the simulated systems. We have chosen the model problem described below – the calculation of the temperature profile in a fluid Argon bounded by two parallel walls in an infinite two-dimensional channel – because the exact (continuum) solution is known for this problem and, additionally, molecular dynamics results have been shown [29, 34] to be in good agreement with the corresponding continuum results for this type of problem.

3.1 Description of Simulations

The dynamics of equations (2.11) and (2.12) were validated using the following nanoscale system: three-dimensional fluid Argon in an infinite 2-dimensional channel bounded by two parallel walls (see Fig. 3-1) heated uniformly. A two-dimensional projection of the (three-dimensional) simulation cell is shown in Fig. 3-2

Two parallel, isothermal, fcc structured walls in the $x-y$ plane are introduced and serve as energy sinks. They allow the simulation to reach a steady nonequilibrium state by effectively imposing temperature boundary conditions on the fluid Argon. Their combined thickness (along the z-direction) is greater than the interaction po-

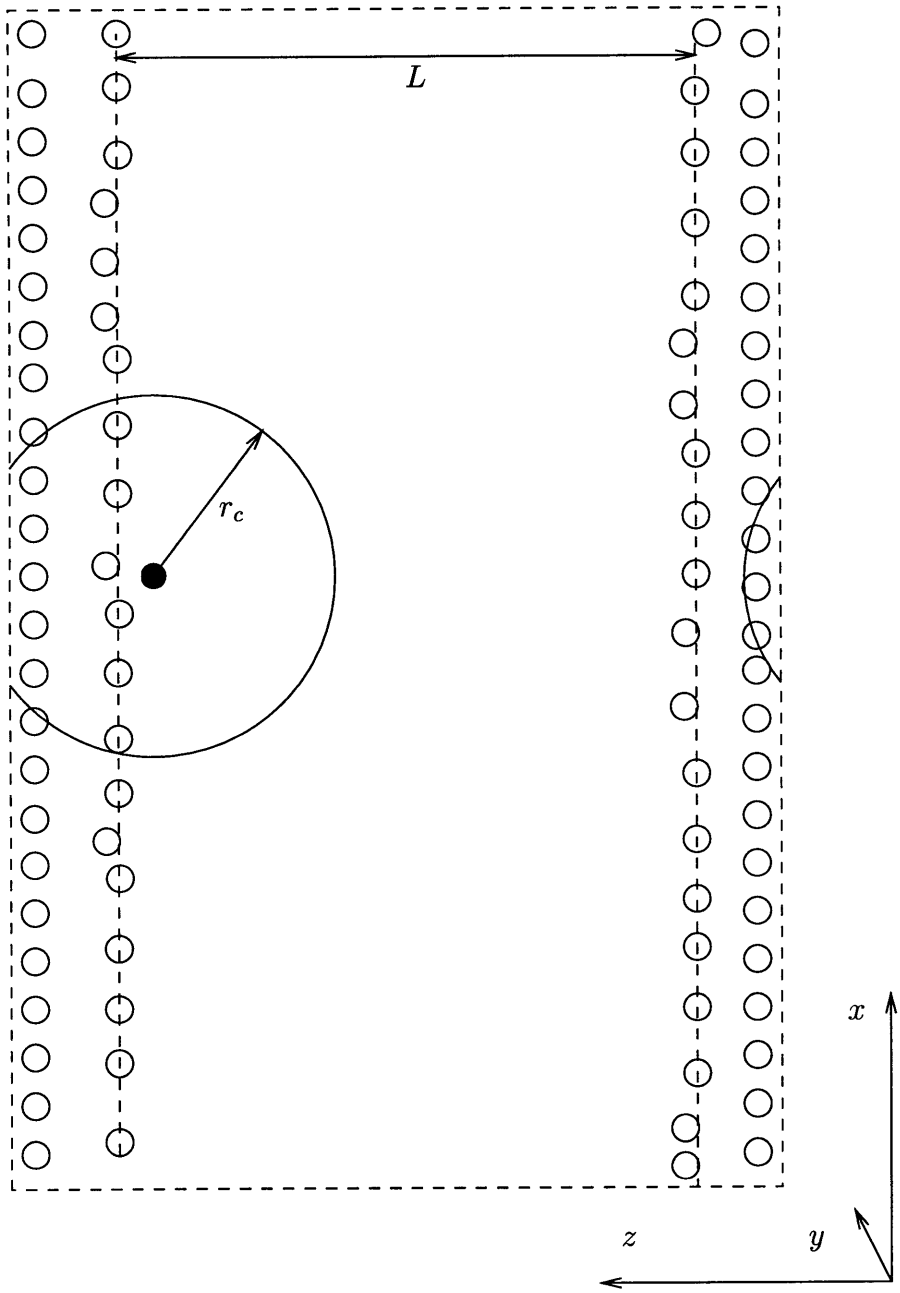

Figure 3-1: System geometry.

tential cutoff (r_c) so that the fluid molecules do not see their images across the walls as shown in the geometry sketch of Fig. 3-1. Both the fluid and the walls are modelled by the well known Lennard-Jones potential. The wall and wall-fluid potential parameters are: $m_W = 2m_{Ar}$, $\varepsilon_W = 5\varepsilon_F$, $\sigma_W = 0.7\sigma_{Ar}$, $\varepsilon_{WF} = 0.02\varepsilon_F$, $\sigma_{WF} = 0.7\sigma_{Ar}$. They do not represent any known solid material. They were chosen as a good compromise between the requirements of minimum number of wall molecules, a melting point that exceeds the highest temperature encountered during the simulation, and minimum layering of the Argon molecules close to the walls. The walls are kept at a constant temperature by rescaling [5] their thermal velocities. This ad hoc procedure does not affect the results of the simulation which are based on the bulk properties of the fluid. We have neglected the fluid state close to the walls in order to ensure that no wall effects contaminated our simulation results.

The simulation proceeds by the numerical integration of the Newtonian equations of motion plus a constant temperature rescaling every two integration timesteps for the wall molecules, and the integration of the constrained equations of motion (2.11, 2.12) for the fluid Argon. We will refer to this simulation prosedure as *case I*, because we have repeated all of our validation simulations using also the rescaling technique of equations (2.15, 2.16). This latter scheme, in summary, consists of the integration of the Newtonian equations of motion (eq. (2.15)) plus a heat addition rescaling step (eq. (2.16)) every two integration timesteps for the fluid Argon, and the integration of the Newtonian equations of motion plus a constant temperature rescaling every two integration timesteps for the wall molecules; we will refer to this scheme as *case II.*

Tests were ran for both *cases* (I and II) at two fluid densities $\bar{\rho} = 0.85$ (480 fluid molecules) and $\bar{\rho} = 0.75$ (416 fluid molecules) and various heating rates. The mean temperature of the simulations depends on the heating rate, the wall temperature and the heat exchange between the walls and the fluid. In order to keep the temperature approximately constant, the temperature of the walls was adjusted accordingly.

In both *cases* (*I* and *II*) a steady state is reached after a short (10000 timesteps) equilibration period. When steady state is reached, samples are taken for a period

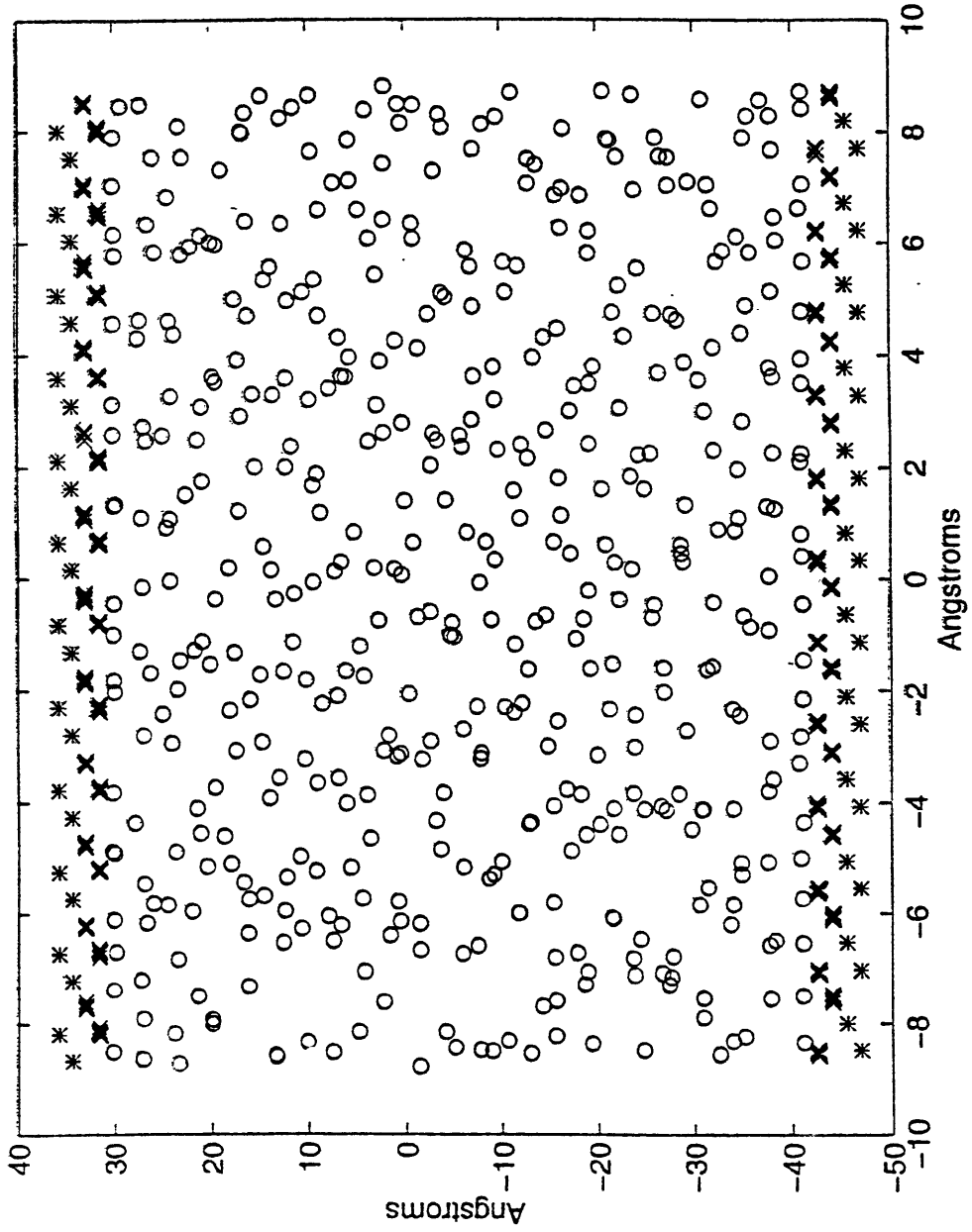

Figure 3-2: Two-dimensional projection of three-dimensional simulation cell.

of 80000 timesteps. The temperature profile is recovered by dividing the fluid region into 12 layers in the z-direction (normal to the walls). These layers are assumed to be in local thermodynamic equilibrium and hence macroscopic properties can be defined over them following the procedure explained in section 2.4. Note that in this problem property variations are expected only in the z-direction and hence the homogeneity of the solution in the x and y directions allows the adoption of slab-like regions that are in local equilibrium. Values for the temperature, density and pressure are evaluated as described in section 2.4. The statistical error in the temperature and density, based on the number of particles in the slabs and the number of timesteps averaged over, is estimated to be ± 0.01 (in reduced units). The results obtained from the two end layers are disgarded because of wall effects. A quadratic least squares fit to the temperature profile gives an estimate for the thermal conductivity of the fluid. Note that a quadratic profile is assumed because, as we show in the next section, the exact solution to the problem at hand can be shown to be quadratic.

3.2 Exact (Continuum) Solution

In this section we derive the continuum solution for the uniformly heated Argon fluid in the two-dimensional channel described above. The hydrodynamic (differential form) energy balance equation can be expressed as

$$\rho c_p \left(\frac{\partial T}{\partial t} + \vec{u} \cdot \nabla T\right) = \nabla \cdot (\lambda \nabla T) + \mu \Phi + \frac{DP}{Dt} + q \tag{3.1}$$

where u is the fluid velocity, c_p is the fluid specific heat, Φ is the viscous heat generation due to the fluid motion, μ is the fluid viscocity, λ is the thermal conductivity, and q is the heat addition per unit volume which can vary as a function of space. In the problem at hand there is no fluid motion and no unsteady effects and hence the equation reduces to

$$\nabla \cdot (\lambda \nabla T) + q = 0. \tag{3.2}$$

Additionally, q does not vary as a function of space and we assume that the temperature variation is too small to have an appreciable effect on the thermal conductivity. We will examine the validity of this assumption in section 3.3. We also note that the solution is homogeneous in the x and y directions, and hence the solution, given that both walls at $z = 0$ and $z = L$ are at $T = T_o$, is

$$T - T_o = -\frac{1}{2}\frac{qz^2}{\lambda} + \frac{1}{2}\frac{qzL}{\lambda} = -\frac{1}{2}\frac{q}{\lambda}z(L - z). \tag{3.3}$$

As we can see the exact continuum solution for the constant heat addition problem with constant thermal conductivity requires a quadratic temperature profile, the curvature of which depends linearly on the heat addition rate and inversely to the thermal conductivity of the material. We will use this fact in section 3.4 to obtain estimates for the thermal conductivity of fluid Argon.

3.3 Error Estimation

The thermal conductivity of fluid Argon at the conditions of the simulation is a very weak function of the temperature, but depends rather strongly on the fluid density. Hence we would expect to have variations of thermal conductivity due to the variable temperature in the solution field. In this section we show that this temperature variation is not enough to cause a significant error in our results which assume an effective thermal conductivity at a mean simulation temperature for the purposes of comparing to the experimental value.

We first like to note that although the temperature dependence of thermal conductivity is very small, this is not true for the thermal conductivity dependence on the fluid density. The fluid density varies according to the equation of state $\rho = \rho(P, T)$ in order to keep the pressure in the fluid constant since no flow is observed, and hence influences the results and the validity of the assumption of constant thermal conductivity introduced in the previous section.

The thermal conductivity has been shown [29] to be fairly well corelated (in the

property region of interest) with temperature and density using the following formula:

$$\lambda = 0.015\left(\exp\left(\frac{0.833\rho}{\rho_c}\right) - 1\right) + \lambda_e \tag{3.4}$$

where

$$\lambda_e = \frac{A\sqrt{T}}{\left(1 + \frac{B}{T}10^{-\frac{C}{T}}\right)}, \tag{3.5}$$

ρ_c is the critical density for Argon, and A, B, C are known constants which result in the weak variation of thermal conductivity with temperature and hence allow us to assume that

$$\frac{d\lambda_e}{dT} = 0. \tag{3.6}$$

To simplify the algebraic manipulation we introduce the compressibility factor

$$Z = \frac{P}{\rho RT}\,, \tag{3.7}$$

and the following first order expansion for the ratio ρ/ρ_c,

$$(\frac{\rho}{\rho_c})|_T \simeq (\frac{\rho}{\rho_c})|_{T_o} + \frac{\partial}{\partial T}(\frac{\rho}{\rho_c})|_P(T - T_o) \tag{3.8}$$

$$(\frac{\rho}{\rho_c})|_T \simeq (\frac{\rho}{\rho_c})|_{T_o} + \frac{\partial}{\partial T}(\frac{Z_c T_c}{ZT})\,(T - T_o) = (\frac{\rho}{\rho_c})|_{T_o} + \alpha(T - T_o)\,, \tag{3.9}$$

where state o is a reference state (equilibrium state of unheated fluid), $(\frac{\rho}{\rho_c})|_P$ means evaluated at constant pressure, $\alpha \simeq -0.009K^{-1}$, and all numerical values have been computed from tables [1] at state o. Note that the numerical values introduced in this section refer to the simulation case with fluid density $\rho = 0.85$. The numerical values of the constants are slightly different for the case where $\rho = 0.75$ but cannot, by any means, alter the conclusions of this section.

Defining $b = 0.015$, $c = \exp(\frac{0.833\rho_o}{\rho_c})$ we have

$$\lambda = b\,c\,\exp(a(T - T_o)) - b + \lambda_e \tag{3.10}$$

where $a = 0.833\alpha$ and our heat balance equation (eq. (3.2)) becomes

$$\frac{d}{dz}(b\,c\,\exp(a(T-T_o)) - b + \lambda_e)\frac{dT}{dz}) = -q \tag{3.11}$$

Linearizing $b\,c\,\exp(a(T-T_o))$ for $|a(T-T_o)| \simeq 0.09 \ll 1$, solving for $(T-T_o)$, and applying the boundary conditions of section 3.2, we obtain

$$\frac{1}{2}a\,b\,c(T-T_o)^2 + \lambda_o(T-T_o) = -\frac{1}{2}\,q\,z^2 + \frac{1}{2}q\,z\,L \tag{3.12}$$

where $\lambda_o = b\,c - b + \lambda_e$. If we denote

$$\frac{1}{2}q\,z^2 - \frac{1}{2}q\,z\,L \equiv \chi(z) \tag{3.13}$$

such that the previous solution (equation (3.3)) can be written as

$$T - T_o = -\frac{\chi(z)}{\lambda}, \tag{3.14}$$

we have

$$T - T_o = \frac{-\lambda \pm \sqrt{\lambda^2 - 2\,a\,b\,c\,\chi}}{a\,b\,c} \tag{3.15}$$

which can be linearized (for small $\frac{a\,b\,c\,\chi}{\lambda^2}$ ($\max_z \frac{a\,b\,c\,\chi(z)}{\lambda^2} < 0.02$)) to

$$T - T_o = -\frac{\chi(z)}{\lambda}(1 - \frac{a\,b\,c\,\chi(z)}{\lambda^2}). \tag{3.16}$$

Note that we have also rejected the negative solution.

We can now check whether the variable thermal conductivity introduces significant differences in the solution. We will use the fact that in our simulations

$$(T - T_o)|_{max} = -\frac{\chi(z = L/2)}{\lambda} \tag{3.17}$$

will be of the order of 0.08, and subsequently calculate the percentage change in this

maximum value which is given by eq. (3.16) as

$$-\frac{a\,b\,c\,\chi(z=L/2)}{\lambda^2} \simeq -1\%. \tag{3.18}$$

As we can see, the change is negligible and hence our assumption of negligible effect of the thermal conductivity variation on the solution is valid.

3.4 Results

Fig. 3-3 shows one example of the temperature profile obtained in our simulations. The solid line represents the least-squares fit to the data from the ten inner slabs, from which the thermal conductivity is estimated. As explained in section 2.4, the variation due to the temperature gradient in this layer is smaller than the statistical variation in this region of space expected from ensemble theory. Due to the homogeneity of the solution in both the longitudinal direction (x) and the direction into the paper (y), these regions have the shape of slabs of thickness 1.8σ.

Table 3.1 reports the estimates for the thermal conductivity λ obtained from the curvature of the temperature profile at the operating conditions indicated. Agreement with experimental data is good. The thermal conductivity estimates are well within the rather strict estimation of the expected error in the simulation (10%). Simulations on similar systems have shown [29] that MD simulations using Newton's equations (eq. (2.1)) give estimates for the thermal conductivity in agreement with the experimental data in [1], but also exhibit relatively large uncertainties. We can also observe that the thermal conductivity estimate for *case II* tends to be higher than for *case I*. This, however, is not always true and the variation is well within the estimated error. We thus conclude that no systematic deviation exists.

The previous tests have shown that the equations of motion introduced in section 2.3 can be used to simulate constant heat addition to a fluid without adversely affecting its statistical mechanical properties. Further confirmation of this result comes from the constant pressure evaporation simulations described now.

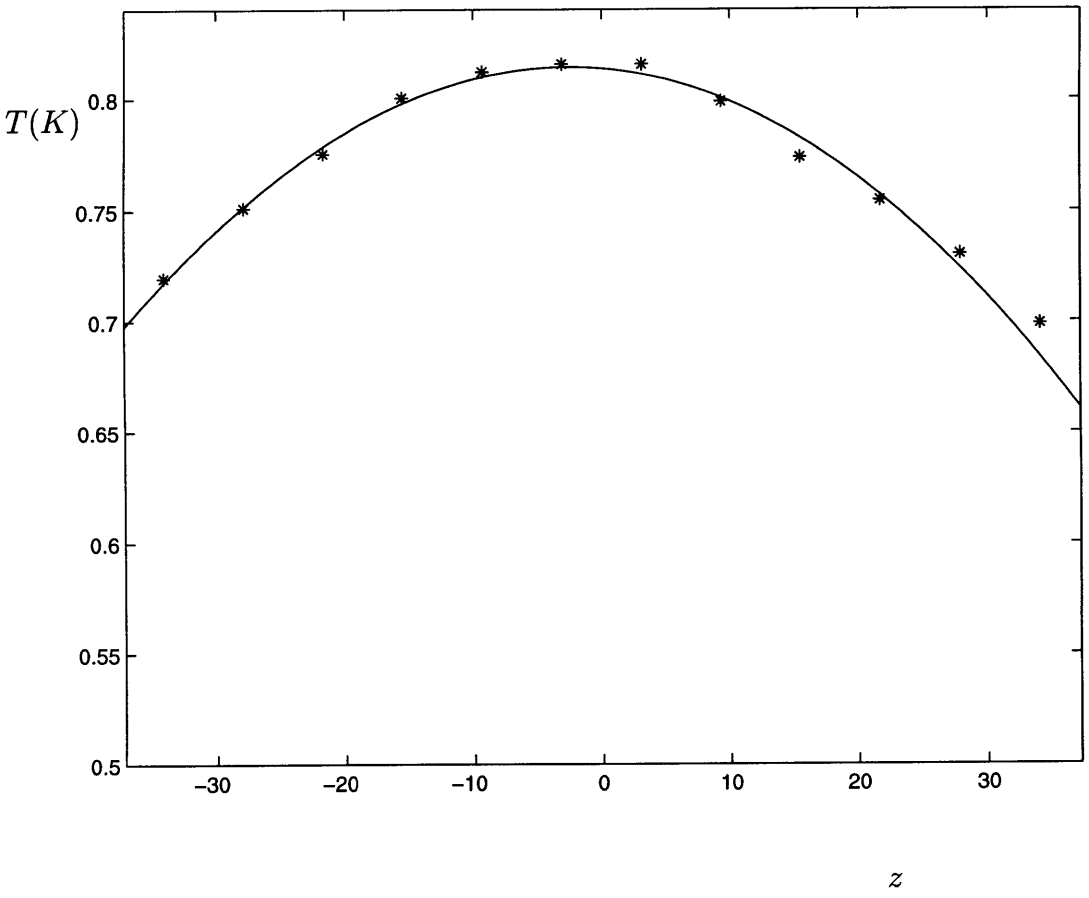

Figure 3-3: Temperature as a function of transverse direction (z) for case I, $\dot{Q} = 2.5 \times 10^{-3}$, $\bar{\rho} = 0.855$. The solid line shows a least squares fit to the data from the ten inner slabs. Walls at $z = 39$, $+39$. Dimensions in Å. The layers close to the walls (at $z = -33$, $+33$) are disgarded because of wall effects.

$\bar{\rho}$	$\bar{T}$	λ	λ_e	Case	$\dot{E}$
0.745	1.04	0.71	0.77	I	3.125×10^{-3}
0.745	1.04	0.83	0.77	II	3.125×10^{-3}
0.74	1.16	0.78	0.77	I	4.6875×10^{-3}
0.74	1.16	0.86	0.77	II	4.6875×10^{-3}
0.74	1.28	0.74	0.77	I	6.25×10^{-3}
0.74	1.28	0.74	0.77	II	6.25×10^{-3}
0.855	0.78	0.95	0.99	I	2.5×10^{-3}
0.855	0.78	1.02	0.99	II	2.5×10^{-3}
0.855	0.83	1.08	0.99	I	3.125×10^{-3}
0.855	0.83	1.05	0.99	II	3.125×10^{-3}
0.845	0.96	1.00	0.97	I	4.6875×10^{-3}
0.845	0.96	1.03	0.97	II	4.6875×10^{-3}

Table 3.1: Comparison between simulation and experiment for the thermal conductivity. $\bar{\rho}$ (± 0.01) and $\bar{T}$ (± 0.01) are mean simulation density and temperature; λ (± 0.1) is simulation thermal conductivity from least squares temperature profile; λ_e (± 0.05) is experimental value of conductivity at $(\bar{\rho}, \bar{T})$. The sources of error for λ_e are the error in P, T and the error in the fitting formula for the experimental data.

Chapter 4

Constant Pressure Evaporation Simulations

In this chapter we present simulations of the evaporation of fluid Argon clusters at constant pressure. The heat addition method has been validated in the previous chapter and we thus expect that the dynamics observed will not be contaminated by adverse effects resulting from the constrained equations of motion. We will additionally compare our results with already existing results for the equilibrium phase change properties of fluid Argon, both from experiments and numerical simulations. To the author's knowledge, this is the first time-dependent simulation of phase change using MD. Previous work has been limited to "mapping" the phase diagram through quasistatic simulations, which therefore implicitly assumed that time-dependent simulations sample a path through the phase diagram that consists of the (quasi-)equilibrium results obtained through equilibrium simulations.

4.1 The Evaporation Simulations

We first describe the baseline calculation of this section: all simulation parameter values can be assumed to be as defined in this baseline, unless otherwise specified. A cluster of 480 Argon atoms is thermally equilibrated at constant pressure ($P = 0.07\varepsilon/\sigma^3$) and zero heat addition ($\lambda = 0$) for a period of 320 τ. The simulation

box is initially cubic with side $\Lambda = 8.95\sigma$ ($\rho = 0.67\sigma^{-3}$) and fully periodic. The "fictitious" mass parameter of the pressure reservoir (W) is set to $2.5m$. (We have verified that the results of our simulations do not change significantly if we decrease W by an order of magnitude. Increasing W slows the response of the system and produces large pressure variations around the desired value. For this reason results for $W = 25m$ were considered unreliable.)

After the equilibration period, the exact equations of heat addition (2.11) and (2.12) are integrated to simulate heating of the fluid at the same constant pressure with $\dot{Q} = 3.125 \times 10^{-3}\varepsilon/(m\tau)$. Thermodynamic properties as a function of time are defined as averages of the corresponding appropriate microscopic quantities (as defined for example in [29]) over intervals of 16τ. We also present some results obtained using equations (2.15) and (2.16) during the heat addition phase, but it is implied that unless otherwise stated, the results shown will be from the integration of equations (2.11) and (2.12).

Finally the evaluation of macroscopic properties (energy E, temperature T, pressure P, and density ρ) follows from the usual definitions for statistical mechanical systems introduced in section 2.4. All extensive properties (energy E, heat addition rate $\dot{Q}$, entropy S, and Gibbs free energy G) will be given in specific (per unit mass) reduced units.

4.2 Results

Fig. 4-1 shows the temperature, and density of the fluid as a function of time after the initiation of heating. We will use Fig. 4-1 to define points A, B, C, D, F, H, and I which we will refer to in the rest of the paper. Point A denotes the start of the heat addition; B signifies the point at which the temperature first reaches the saturation temperature (for the simulation pressure) as given by equilibrium simulations [2]; C denotes the local maximum temperature overshoot; at D the temperature is again equal to the saturation temperature after reaching the maximum at C; F denotes the local minimum temperature following C; H denotes the point at which the temper-

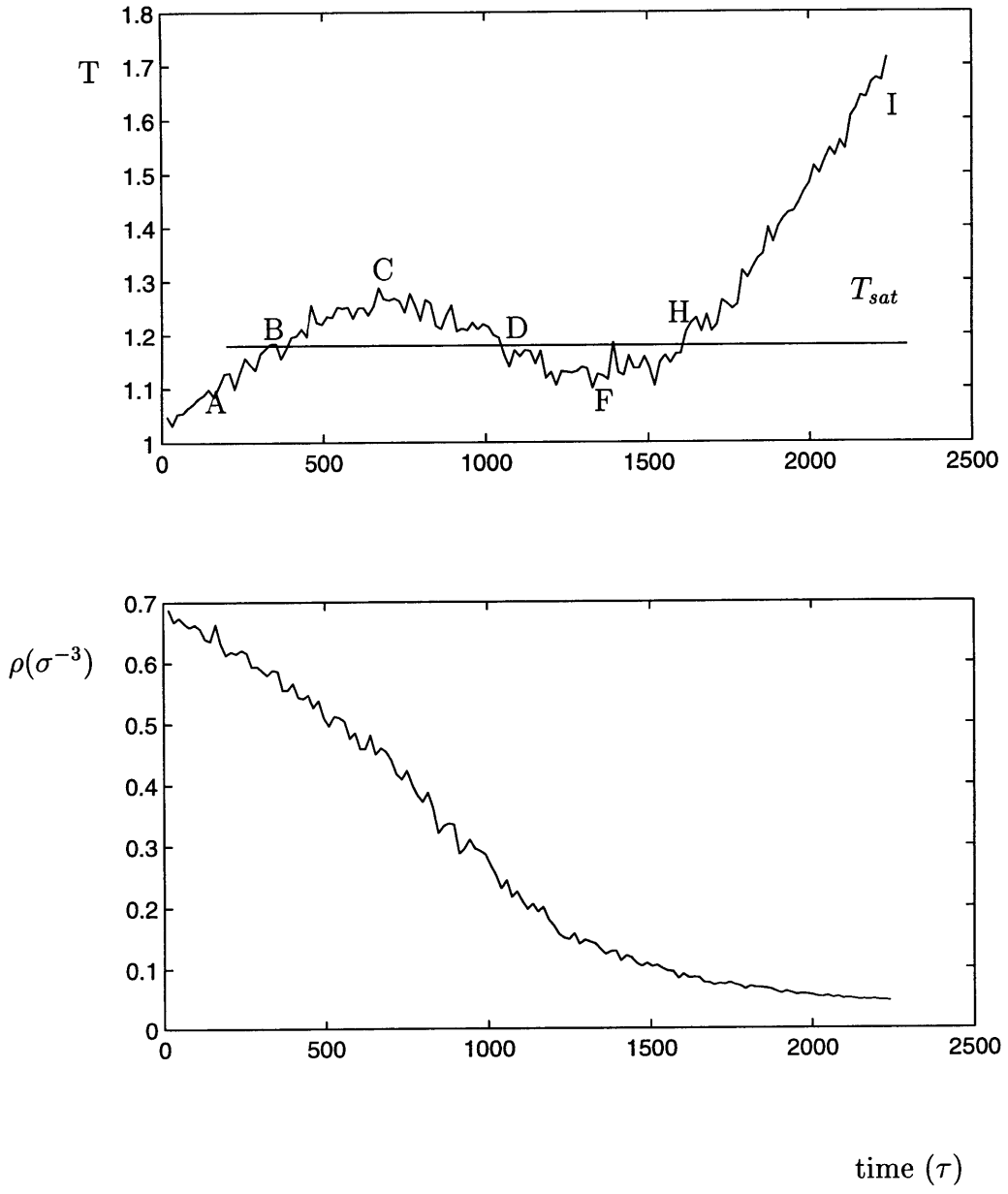

Figure 4-1: Temperature and density of the fluid as a function of time after initiation of heating. The saturation temperature (T_{sat}) was obtained by a Maxwell construction discussed later, which is in agreement with data from [18].

ature reaches the saturation temperature after the conversion of all liquid to gas; I denotes the end of the simulation.

Fig. 4-2 verifies that the system indeed goes through a liquid-vapor coexistence phase by showing the instantaneous positions for the molecules comprising the system at the times corresponding to points C, D, F, and H. We have also verified that the temperature is reasonably uniform within and between the two phases, to ensure that the above observed behavior is not due to some thermal instability accosiated with the heating mechanism.

Fig. 4-3 shows the numerical integration results for the entropy S and the Gibbs free energy $G = E - TS + PV$ as a function of temperature. S is evaluated by numerical integration of

$$S_Z = S_A + \int_A^Z \frac{dQ}{T} = S_A + \int_A^Z \frac{d(E+PV)}{T} \tag{4.1}$$

along the system path starting from A; here Z is any point on the system path. Since the integration does not need to be evaluated from both phases, the initial entropy and, as a result, the Gibbs free energy datum can be set arbitrarily. The entropy is set equal to zero at A (start of heating). The entropy of the fluid for simulations at a different pressure (introduced later) is determined consistently with the datum defined above, by using data from [1] to find the difference in entropy between the initial states of the various simulations at the different (constant) pressures. Note that this integration assumes that the deviation from equilibrium is negligible, or alternatively that the heat added to the system is thermalized in a timescale smaller that the heat addition timescale, as discussed in section 2.

The results of Fig. 4-3 are consistent with the findings of other researchers [4, 12, 2]. Although the results reported in these studies exhibit van der Waals type loops in the $P - V$ diagram (constant temperature simulations), it is well known [3, 19] that the van der Waals equation produces loops in both the $P - V$ and $T - S$ diagrams with the characteristic feature observed in Fig. 4-3 of the Gibbs free energy (G) "crossing back on itself" under both constant temperature and constant pressure projections.

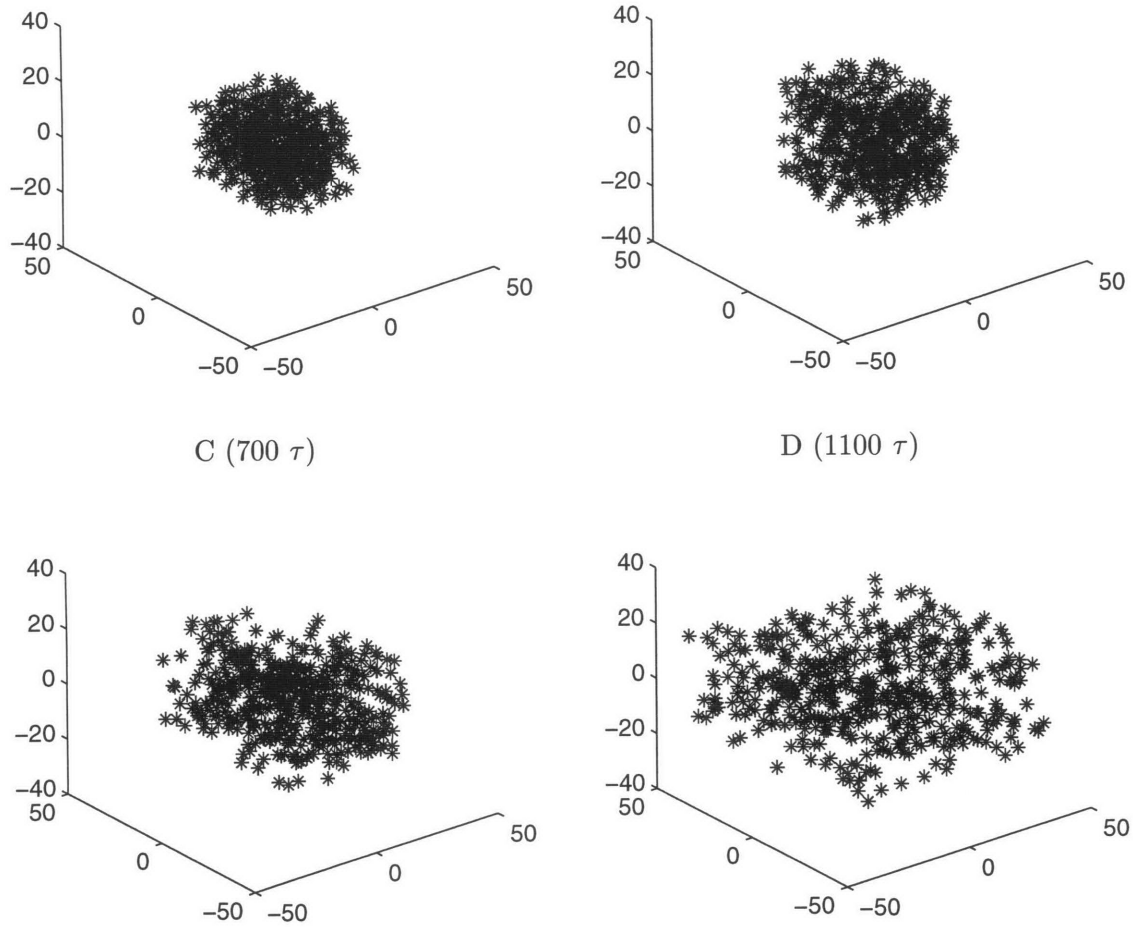

Figure 4-2: Instantaneous molecular positions at the indicated times. Dimensions in Å.

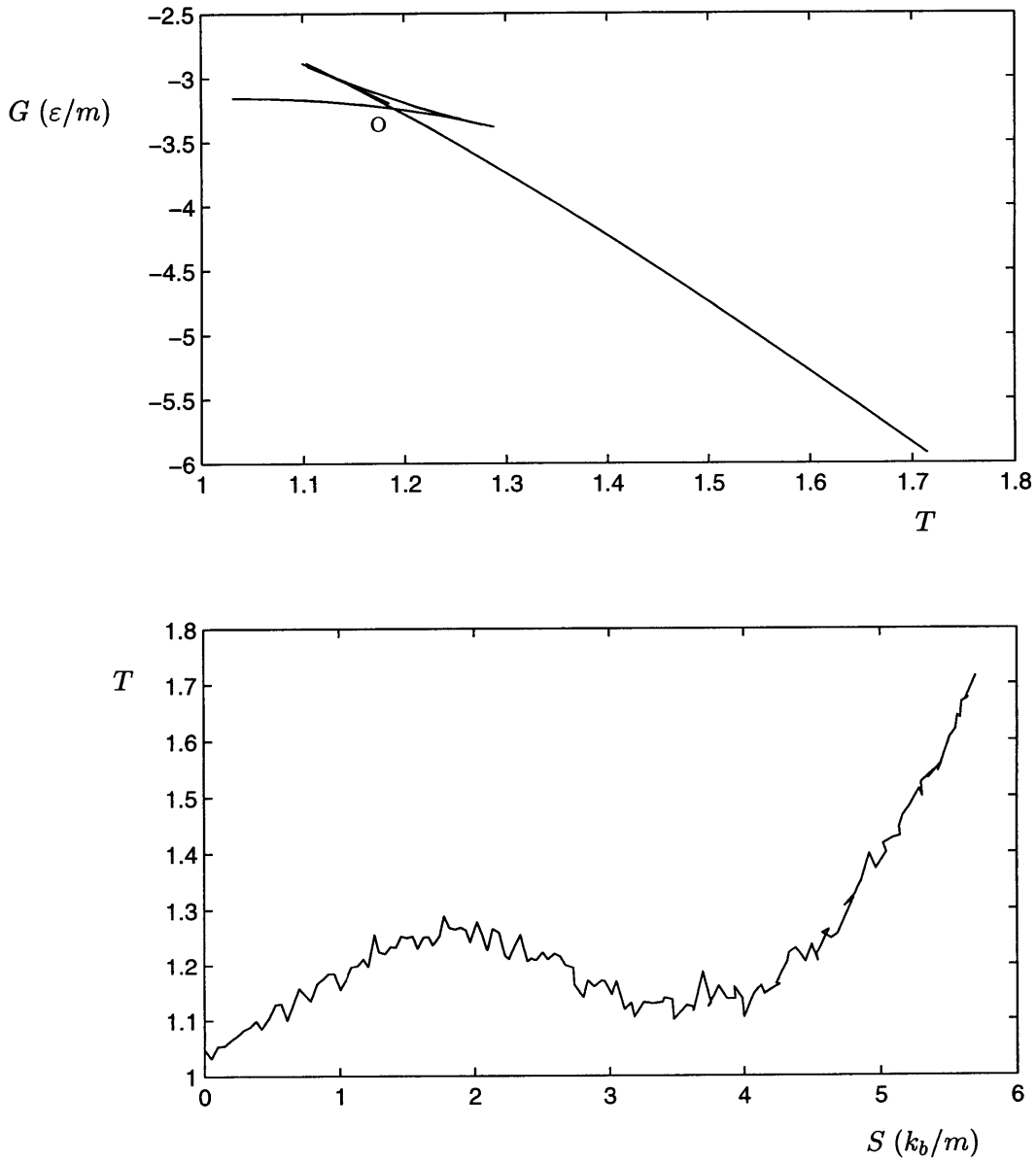

Figure 4-3: Gibbs free energy as a function temperature (top) and temperature as a function of entropy (bottom) during the phase change.

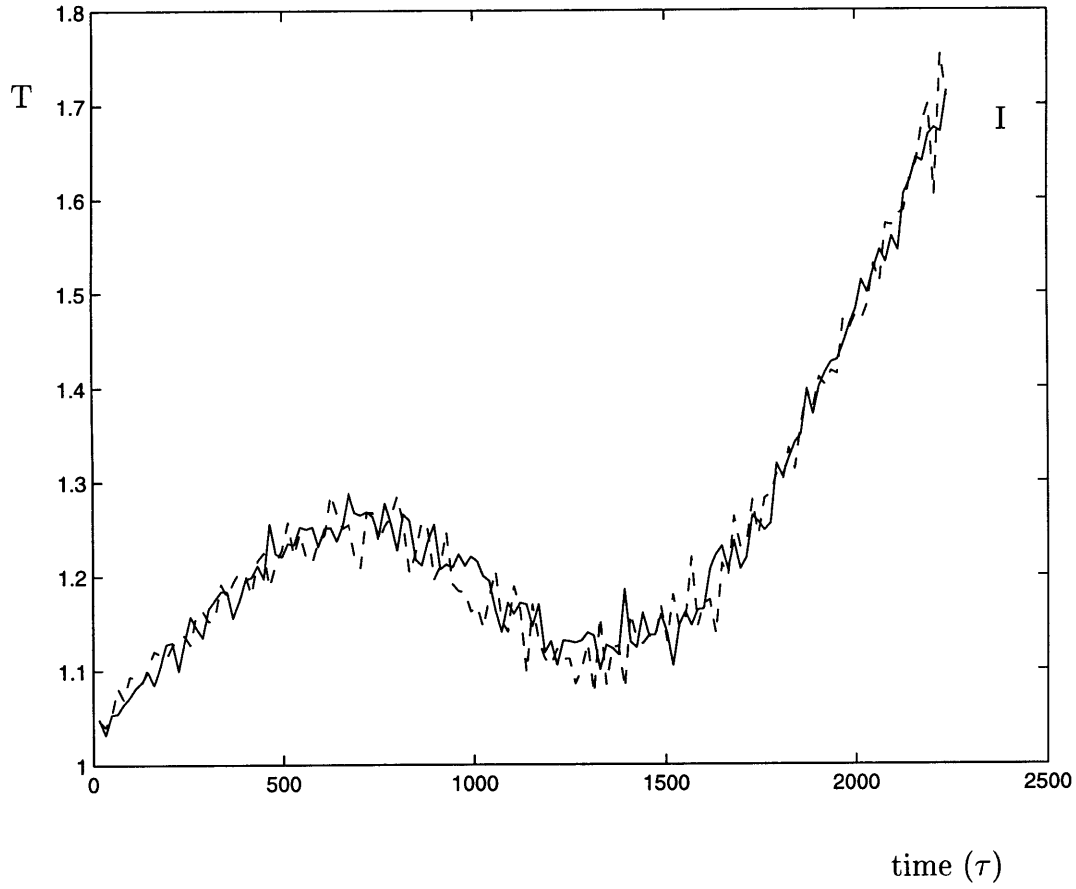

Figure 4-4: Temperature histories for evaporation heating (solid line) and condensation cooling (dashed line). At "I" heat input changes direction and heat is removed from the system. Time increases from right to left for dashed line.

We believe that the quasistatic simulations, in agreement with linear response theory, were sampling the time dependent path of the system recovered by our simulations. To verify this assertion, we use ten equispaced (in time) states on the temperature history of Fig. 4-1 as initial states of simulations with zero heat addition: the fluid is left to evolve for 960τ using the Newtonian equations of motion (equation (2.11) with $\lambda = 0$). The state of the fluid remains invariant during this period of time indicating that (i) the state is not a result of the constrained equations of motion and, (ii) the states between B and H are indeed (metastable) equilibrium states on the path of the liquid-vapor phase transition such as the ones sampled by previous quasiequilibrium simulations.

We also present simulations of cooling ($\dot{Q} = -3.125 \times 10^{-3} \varepsilon/(m\tau)$) of the resulting vapor phase (state I). The cooling curve (dashed line in Fig. 4-4) is superposed on the heating curve (solid line in the same Figure), for comparison purposes; as a result, time for the cooling curve increases from right to left. The reversible behavior observed reinforces the belief that the observed $T - S$ diagrams contain a dynamical signature of phase change. We would like to note that the integration of equations (2.11) and (2.12) displays very slow convergence characteristics for the case of heat removal ($\dot{Q} < 0$) and as a result we use the rescaling procedure (eqs (2.15) and (2.16)) for the heat removal simulations. To verify that the two methods are equivalent we have compared the results of the two methods. Fig. 4-5 shows that the results of the two integration methods are indistinguishable to within the statistical uncertainty (± 0.03 in temperature) of our simulations, so that the comparison of Fig. 4-4 is valid.

The saturation temperature, T_{sat}, is defined by point O on the $G - T$ diagram of Fig. 4-3, or equivalently, by a "Maxwell construction" [3] on the $T - S$ diagram of the same Figure. The value obtained ($T_{sat} = 1.18$) is close to the value cited in [23] (1.19) for MC simulations with a cut-off of 2.5σ, the full Lennard-Jones prediction (1.19) of Powles [23], and the (more accurate) MC predictions (1.18) of Lotfi et al. [18]. The saturated liquid density ($0.59\sigma^{-3}$), and saturated gas density ($0.08\sigma^{-3}$), compare very well with the corresponding predictions of Powles [23] which are $0.59\sigma^{-3}$ and $0.12\sigma^{-3}$ respectively, and the predictions of Lotfi et al. [18] which are $0.59\sigma^{-3}$ and

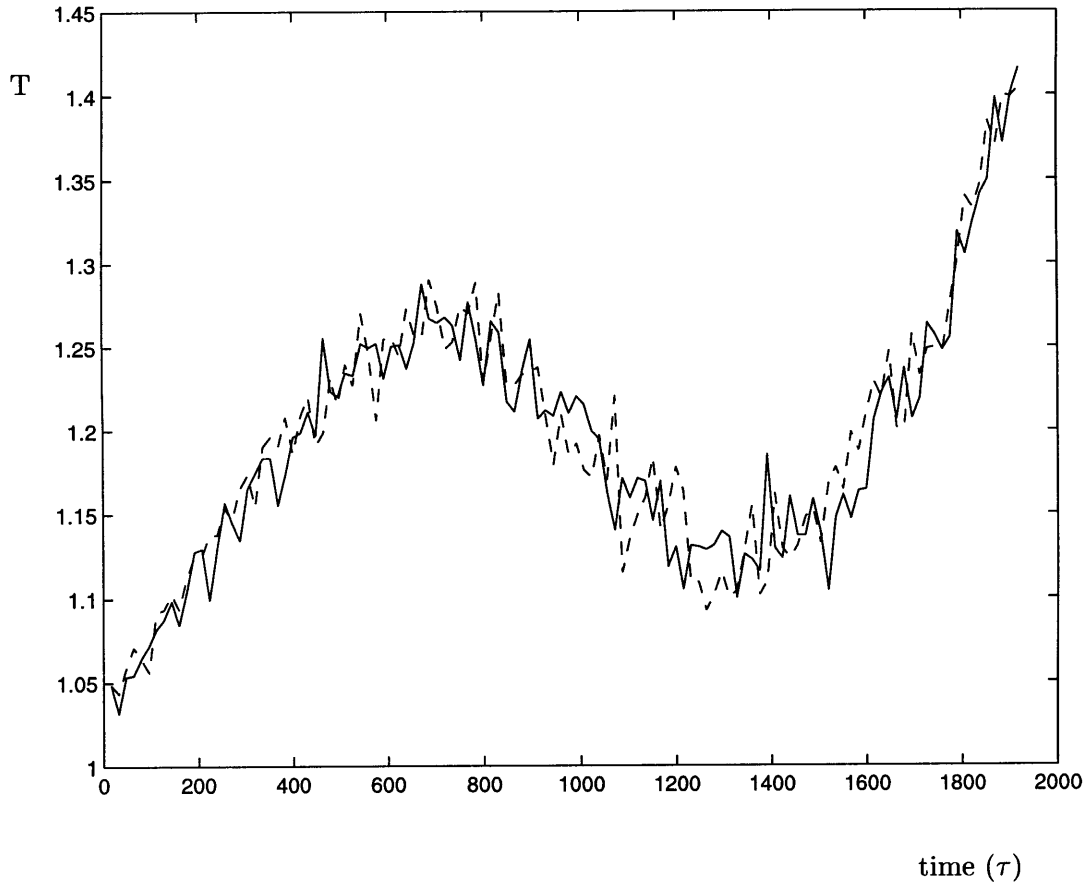

Figure 4-5: Evaporation history using equations (2.11) and (2.12) (solid line) and equations (2.15) and (2.16) (dashed line).

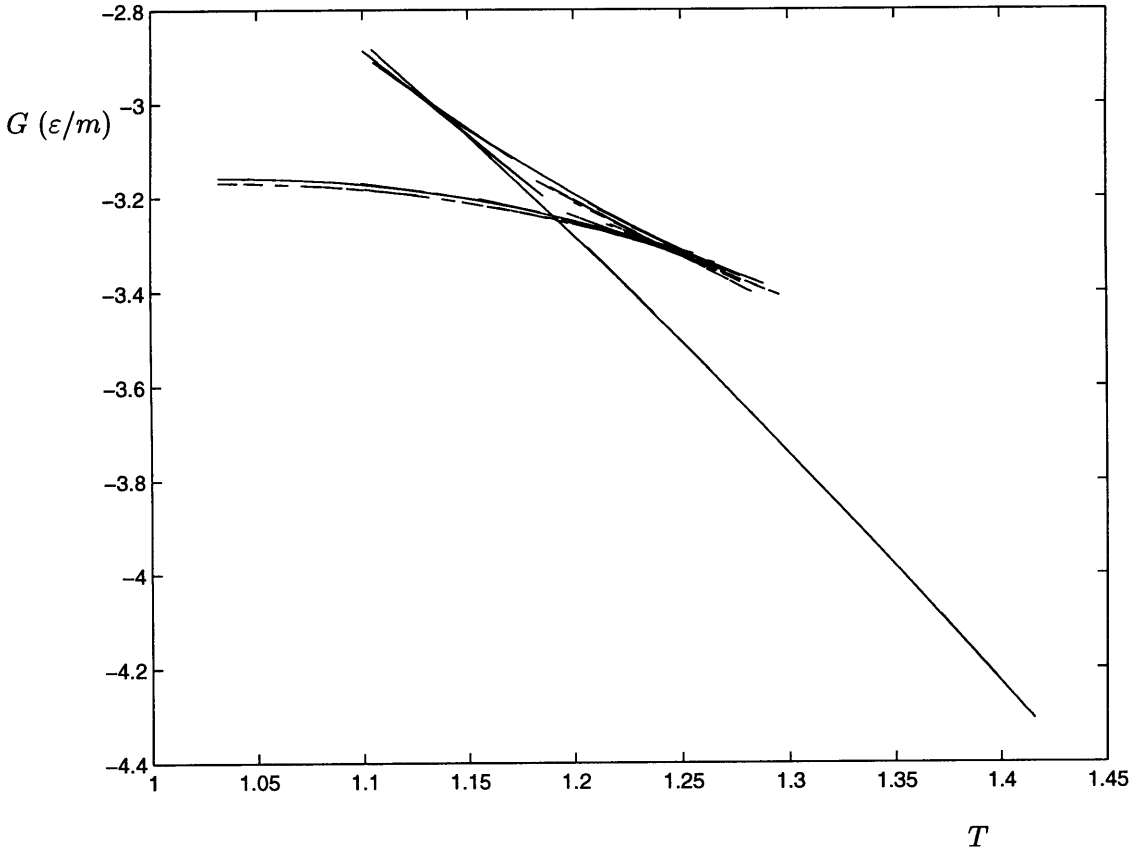

Figure 4-6: Gibbs free energy versus temperature for different heating rates. $\dot{Q} = 3.125 \times 10^{-3}\, \varepsilon/(m\tau)$ for the solid line and $\dot{Q} = 1.5625 \times 10^{-3}\, \varepsilon/(m\tau)$ for the dashed line.

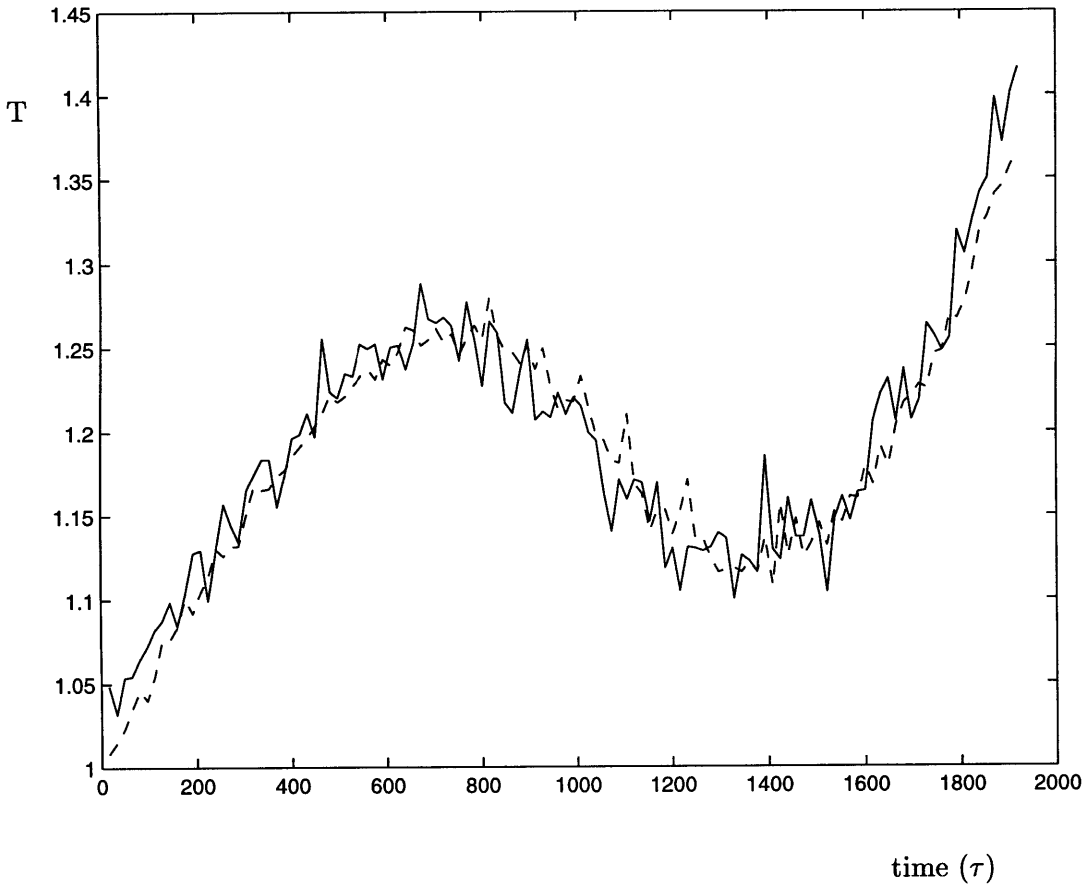

Figure 4-7: Temperature history for different number of molecules (n). n=480 for the solid line, n=1920 for the dashed line.

$0.09\sigma^{-3}$, respectively.

Further evidence that the observed behavior is not related to the heating rate but is a reflection of the path characteristic of phase change in $G - T$ space is offered in Fig. 4-6. The $G - T$ diagrams for different heating rates are identical; time is reduced to the role of a parameter along the path. In the next chapter we show that for homogeneous nucleation the effect of the heating rate is very small and hence, can be neglected for the range of heating rates presented here. Our results are also independent of the number of molecules in the system: the results for 960,

1920, 3840 molecules are all indistinguishable from the results of Fig. 4-1 within the temperature uncertainty of our simulations (± 0.03). This is demonstrated in Fig. 4-7 for simulations with 480, and 1920 molecules. The cases with 960 and 3840 molecules have been omitted for clarity.

Chapter 5

Phase Change Dynamics

Metastable states are encountered in many situations of practical interest; one example is the design of steam turbines where the nucleation of small droplets results in the rapid erosion of the turbine blades and hence rapid loss of efficiency and, ultimately, failure. Materials properties can be greatly affected by their microstructure which, among other things, is influenced by their quench history.

The existense of metastable and unstable states is predicted by various equations of state, resulting both from curve fits of experimental data [17] and theoretical considerations [27, 16]. Skripov [27] argues that in the thermodynamic limit we obtain the most probable macrostate which, however, neglects metastable states induced by surface effects. It has been shown [27] that by considering the surface contributions of the statistical integrals in the thermodynamic limit of a one-dimensional system, the one-dimensional van der Waals equation can be derived.

The theoretical stability considerations for the distinction between metastable and unstable states are summarized in [27, 16]; metastable states are enclosed by the two phase boundary and the spinodal line, whereas unstable states are the ones enclosed by the spinodal and the density axis in Fig. 5-1. Note that the liquid spinodal corresponds to the locus of points corresponding to point C in Fig. 4-1 as pressure varies, and the vapor spinodal to point F of the same Figure.

Metastable states lead to phase separation by nucleation and growth, whereas unstable states lead to phase separation by spinodal decomposition. In the metastable

region finite perturbations (nucleation sites) are required to initiate the phase separation. The deeper the penetration into the metastable region the smaller the size of the required (critical) sites. Inhomogeneities such as walls and cracks in them, macromolecules, or ionized molecules, usually provide sites for the phase change initiation. Depending on the size of these inhomogeneities a certain degree of penetration into the metastable region is required. Thus a fluid upon heating (say), will enter the metastable region and follow the path required by the heating rate imposed until the penetration depth (superheat) is such that the largest nucleation sites are equal to the above critical size. In the next section we outline the classical derivation for the critical size of nucleation sites as a function of the penetration into the metastable region. In the absense of all inhomogeneities the fluid has to rely on statistical fluctuations to generate the required nucleation sites (homogeneous nucleation). The probability of existence of such sites decreases exponentially with their size.

The spinodal represents the boundary between the metastable and the unstable region, or in other words, the spinodal demarkates homogeneous nucleation from spinodal decomposition. Hence the maximum penetration into the metastable region for which nucleation is still expected to occur coincides with the spinodal, or strictly, a point inside the metastable region and infinitessimally away form the spinodal. For this reason spinodal points are usually identified with homogeneous nucleation. Homogeneous nucleation thus corresponds to the *smallest* spontaneously created nucleation site; larger sites would cause phase separation at smaller penetrations, but are statistically much less likely to occur and in practice never do.

The size of the critical honogeneous nucleation site is a function of the material properties. The same is true of the location of the spinodals and the critical wavelengths characterizing spinodal decomposition. One of the unresolved problems to date [7], is the exact process of transition from homogeneous nucleation to spinodal decomposition.

Experimental verification of homogeneous nucleation has been limited to the demonstration of existence of metastable states through both direct experiments and fitted equations of state, and the identification of the liquid spinodal with the ho-

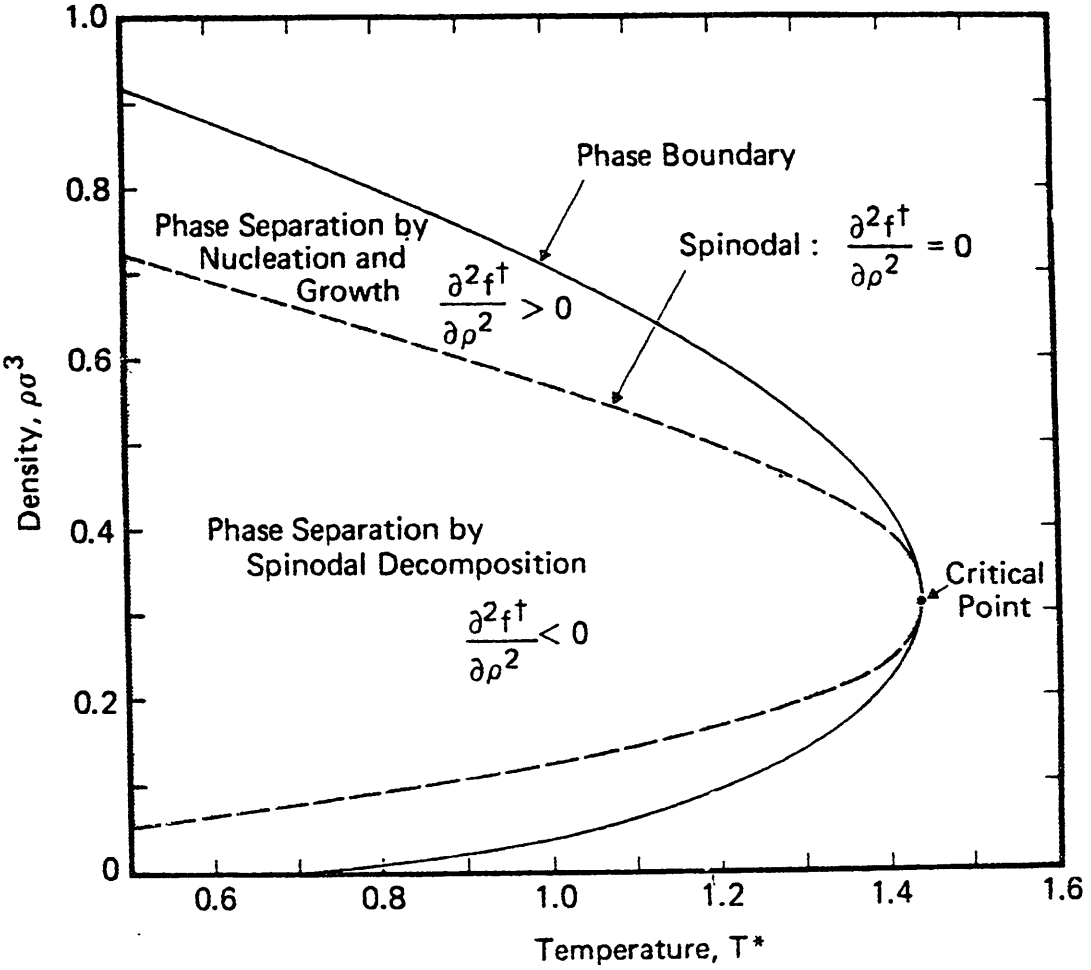

Figure 5-1: Phase boundary and spinodal lines for the Lennard-Jones fluid (from [16]). $f^\dagger$ is the analytic continuation in the two phase region of the Helmholtz free energy density.

mogeneous nucleation limit [17]. The identification of the vapor spinodal with the homogeneous nucleation limit has escaped experimental verification, to the author's knowledge, to date [17]. Because of the impurities and finite size nucleation sites available in real systems, metastable states are difficult to reproduce experimentally; furthermore, no states between the vapor and the liquid spinodal have been experimentally observed.

Our objective is to verify the homogeneous nucleation and stability theory calculations. We will use our maximum supersaturation data (spinodal points C and F) to calculate the critical radii for the homogeneous nucleation limit and show that those are consistent with the length scales and time scales of our simulation. We will also compare the data on the location of the spinodal from our calculation to the results of [16].

5.1 Introduction to Homogeneous Nucleation

We first consider the evaporation case. As the liquid is heated beyond the saturation line (superheated) it becomes energetically favorable for the phase separation to proceed. Vapor bubbles (small clusters of molecules at the vapor density) are formed and collapse continuously such that a steady state of vapor bubble distribution (exponentially decaying in the bubble size) is sustained. At this steady state, the rate of formation of bubbles containing n molecules from growth and collapse of bubbles of $n-1$ and $n+1$ molecules respectively, is balanced by their rate of destruction [28]. Thus the rate of generation of bubbles is uniform accross the size distribution. It is called the nucleation rate J, and is given by [28]

$$\log J(T,P) = a\{1 - e^{[-(T-T_0)G/a]}\}. \tag{5.1}$$

Note that this expession is an approximate curve fit to the various theories that predict nucleation rates, and that a and G are constants that depend on the pressure;

T_0 is the temperature for which

$$\log J(T_0, P) = 0. \tag{5.2}$$

The reader is referred to [27, 28] for more details on the origin of this relation. We can see that the nucleation rate is an exponentially increasing funtion of the supersaturation $(T - T_{sat}(P))$ where P is the pressure of the system.

For phase separation to occur one of the vapor bubbles must grow. The conditions for growth are presented through the following mechanical equilibrium and thermodynamic equilibrium arguments. Alternative arguments (to the mechanical equilibrium) based on energy considerations can be found in [19].

Mechanical equilibrium between a vapor bubble of radius R and the surrounding liquid requires that the pressure inside the bubble P_b be higher than the ambient pressure of the liquid P_l such that

$$P_b = P_l + \frac{2\gamma}{R}\,, \tag{5.3}$$

where γ is the interfacial tension. This equation is known as the Laplace equation. Thermodynamic equilibrium requires that, for the two phases to coexist at the bubble boundary, the temperature of the vapor inside the bubble (which is equal to the temperature of the simulation) be the saturation temperature at the pressure inside the bubble, or

$$T = T_{sat}(P_b). \tag{5.4}$$

Since the saturation temperature is monotonically increasing for increasing pressure we see that the higher the supersaturation $(T - T_{sat}(P))$, and hence the temperature T, the smaller the radius $(R = R_c)$ that satisfies equations (5.3) and (5.4).

In summary, as a fluid is superheated it remains in the metastable state until its temperature increases to a value such that the critical radius corresponding to that state becomes as small as the nucleation sites available. If no external nucleation sites are available the temperature will reach the spinodal value and the fluid will change

phase by homogeneous nucleation. If insufficient time is allowed for the bubbles to nucleate the liquid will cross into the unstable region and phase separation will proceed by spinodal decomposition.

The case for liquid drops forming in a supercooled gas is exactly analogous. In this case, however, energetic arguments [9] show that a liquid drop has a vapor pressure P_v given by

$$\ln(\frac{P_v}{P_\infty}) = \frac{2\gamma}{R\rho_l kT} \tag{5.5}$$

where ρ_l is the liquid drop density, k is Boltzmann's constant, and P_∞ is the thermodynamic limit saturation pressure for the system temperature, that is $P_\infty = P_{sat}(T)$. This equation is known as the Kelvin equation. Mechanical equilibrium requires that the vapor pressure of the drop has to be equal to the pressure of the ambient vapor (P). The pressure of the liquid inside the drop is P_∞ and the thermodynamic equilibrium requires that the supercooling temperature equal $T = T_{sat}(P_\infty)$. All system properties are evaluated at T.

Experimental results [27] for liquid superheating report critical bubble sizes of the order of 70Å with average droplet lifetimes of the order of seconds for materials such as n-pentane, and benzene. Argon experiments indicate that critical bubbles of the order of 35Å can be achieved. We expect that MD simulations would predict smaller (or at most equal) critical radii due to the intrinsic purity, homogeneity and lack of external disturbances in such simulations.

5.2 Simulations and Data Analysis

We perform simulations as described in chapter 4 for different values of the simulation pressure (Fig. 5-2). Our objective is to investigate the ability of nucleation theory to explain the behavior discussed in chapter 4. Using the values of maximum superheat (point C) we attempt to extract estimates of the critical radii of gas bubbles required for homogeneous nucleation to commence. In other words, we will use T_C to find the pressure in the critical bubbles P_b by using $T_C = T_{sat}(P_b)$. This will subsequently yield R_c, the critical bubble radius, through equation (5.3).

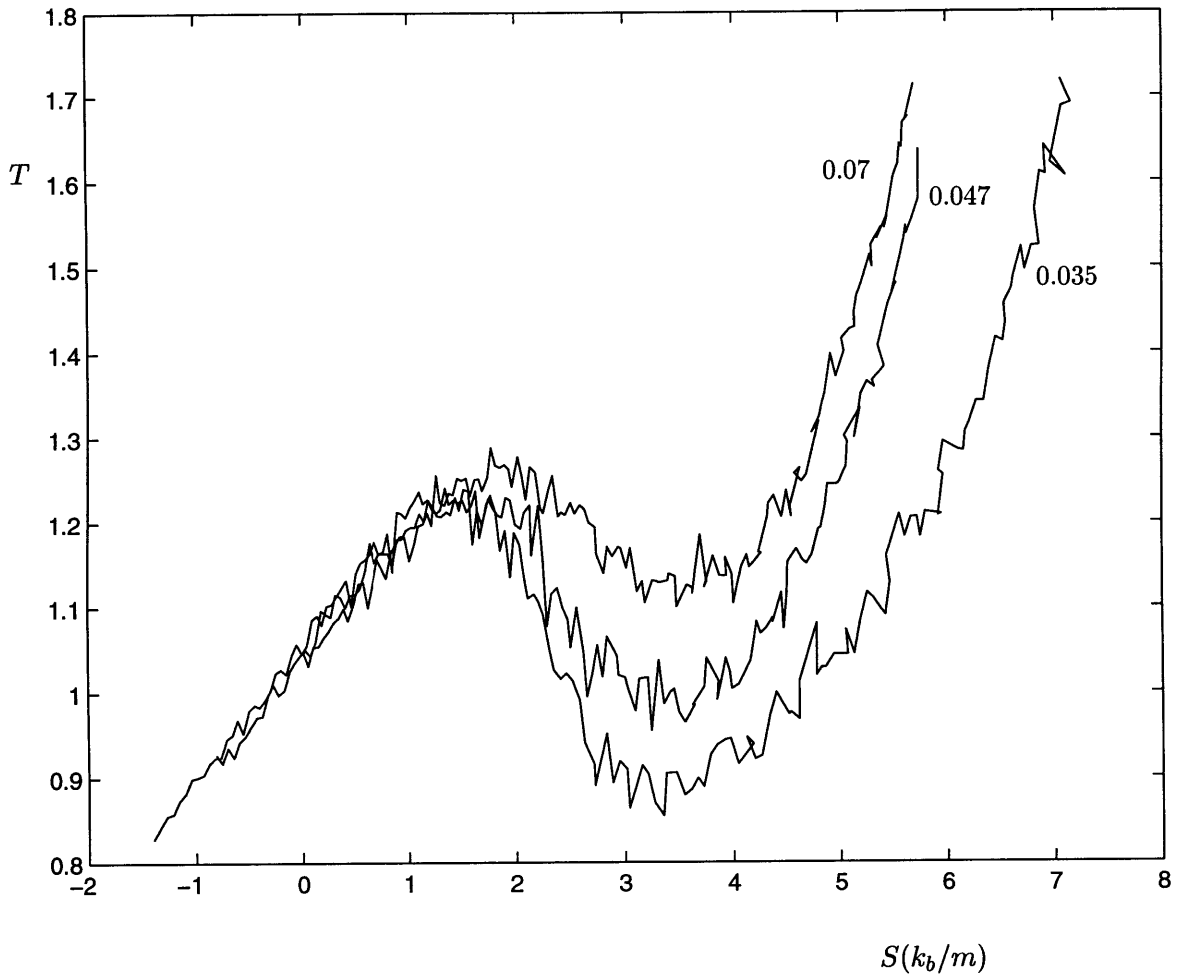

Figure 5-2: Temperature as a function of entropy for the three different pressures (in ε/σ^3). The initial entropy for all three simulations is determined as explained in chapter 4.

Similarly, using the maximum subcooling required (point F) we estimate the critical radius of liquid embrya required for condensation to occur. We estimate P_∞ from T_F through the thermodynamic equilibrium requirement $T_F = T_{sat}(P_\infty)$. The identification of $P_v = P$ in equation (5.5) allows for the solution for the critical radius R_c.

5.2.1 Thermodynamics of Small Clusters

Experimental results and preliminary calculations indicate that the critical clusters (bubbles and drops) are of molecular dimensions. For this reason we need to account

for the dependence of the thermodynamics of these clusters on their size, since both the Laplace and the Kelvin equation have been derived with the use of continuum concepts whose validity is questionable at the molecular scale.

The properties of nanodroplet systems (liquid drop surrounded by vapor) have been investigated by various authors [31, 24, 35] but the results are by no means exhaustive. It has been verified through simulation [31, 35, 25] that Laplace's equation can be used to describe the pressure differential across the interface of a very small droplet with the following refinements imposed by the small size of the drop. First, the droplet radius (R) is identified with the radius of tension of the droplet (R_s), and second, γ is interpreted as the interfacial tension for a curved interface and is properly evaluated at the large curvature of these small droplets. The Tolman equation [32]

$$\gamma = \gamma_\infty (1 + \frac{2\delta}{R_s})^{-1} \tag{5.6}$$

was found [31, 35] to adequately describe the variation of the surface tension for a curved surface (γ) with the radius of tension of the droplet, given the value of the surface tension for a planar interface (γ_∞). The radius of tension (R_s) of the droplet is related to the radius of the equimolar surface of the droplet (R_e) by

$$\delta = R_e - R_s > 0. \tag{5.7}$$

The radius of the equimolar surface (R_e) is the best measure of the size of the droplet and the number of molecules it contains. It can be visualized with the aid of a hypothetical liquid drop-vapor system that has the same number of molecules as the real system. The equimolar surface is the boundary of a hypothetical liquid drop whithin which the density is constant and equal to the central (limiting) density of the real drop. On the vapor side of the boundary, the density decreases discontinuously to a constant value equal to the vapor density at infinity, or sufficiently far from the drop, in the real system [4].

Simulation results for δ reveal some uncertainty as to what its exact value is. Matters are complicated by the apparent dependence of δ on the cut-off radius and

the simulation temperature. The value of 0.8σ adopted here follows the work in [31] and [25] and falls between the extreme values of 0.5σ and 2σ reported in [24] and [35] respectively.

Thompson et al. [31] find that the Kelvin equation is not usefull in describing nanodroplet phenomena. This conclusion is based on their results (reproduced here in Fig. 5-3) that indicate that the limiting form of the Kelvin equation (without the Tolman correction and the introduction of the radius of tension) is in better agreement with their MD results (circles) than the fully corrected results (solid line). Additionally, Powles et al. [24] suggest the use of the Kelvin equation without including the Tolman correction to the surface tension. This is again based on their results (reproduced here in Fig. 5-4) which show that the introduction of a Tolman correction makes agreement between theory and simulation worse. Following the above observations we decided not to use the Tolman equation as a correction for the effects of curvature on the surface tension (for both evaporation and condensation) of the two phases, and hence interpret R as the equimolar radius (R_e) and not the radius of surface of tension (R_s).

For the evaporation case, we remark that the Tolman equation has been derived and validated only for liquid drops surrounded by vapor, and as such it cannot be used for the case of a vapor bubble surrounded by a superheated liquid. Additionally, the vapor bubble radii shown in the results section are large enough that, even if a Tolman type equation would be valid, assuming that $\delta = 0.8$, the correction introduced would be of the order of 10%. This error was considered reasonable given the significant statistical error inherent in [31, 24, 35, 25].

In the condensation case, the resulting liquid radii are significantly smaller and as remarked by Tolman [32], Thompson et al. [31], and Powles et al. [24], the validity of this equation is at least questionable for such small droplets. Most importantly, as shown above, the simulation results of Thompson et al. show that the uncorrected Kelvin equation (not subjected to a Tolman correction) can be used to relate the *equimolar radius* and the vapor pressure of the simulated droplets. In a similar fashion, Powles et al. [24] show that the inclusion of a Tolman correction to the

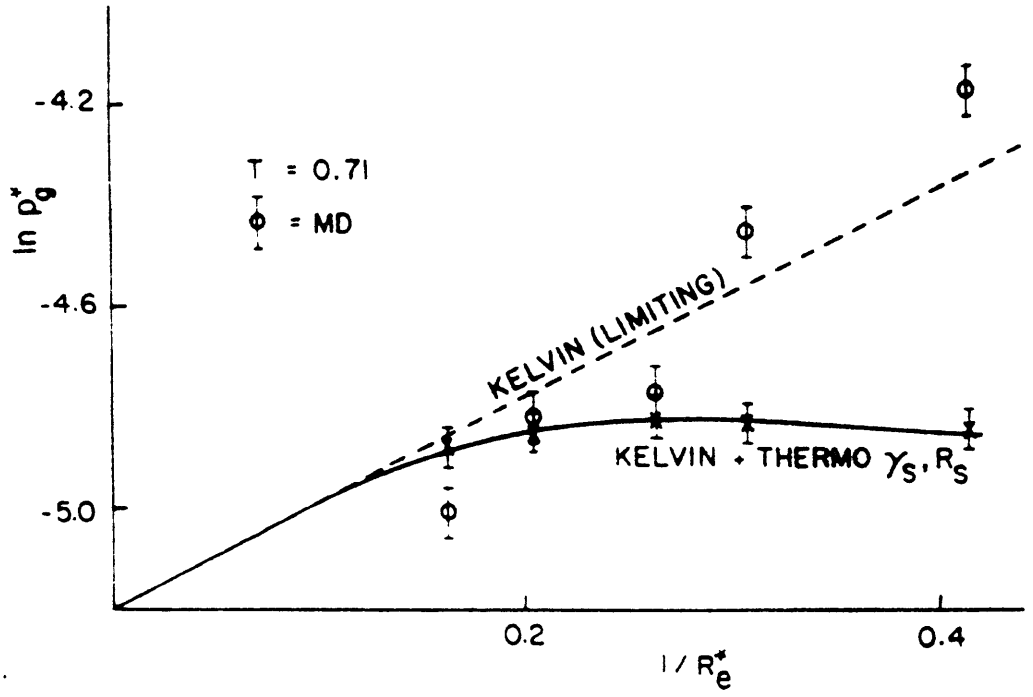

Figure 5-3: Simulation results from [31] for $T = 0.71$ and $\rho \simeq 0.8$. The dashed line denotes the uncorrected results and the solid line shows the results including a Tolman correction.

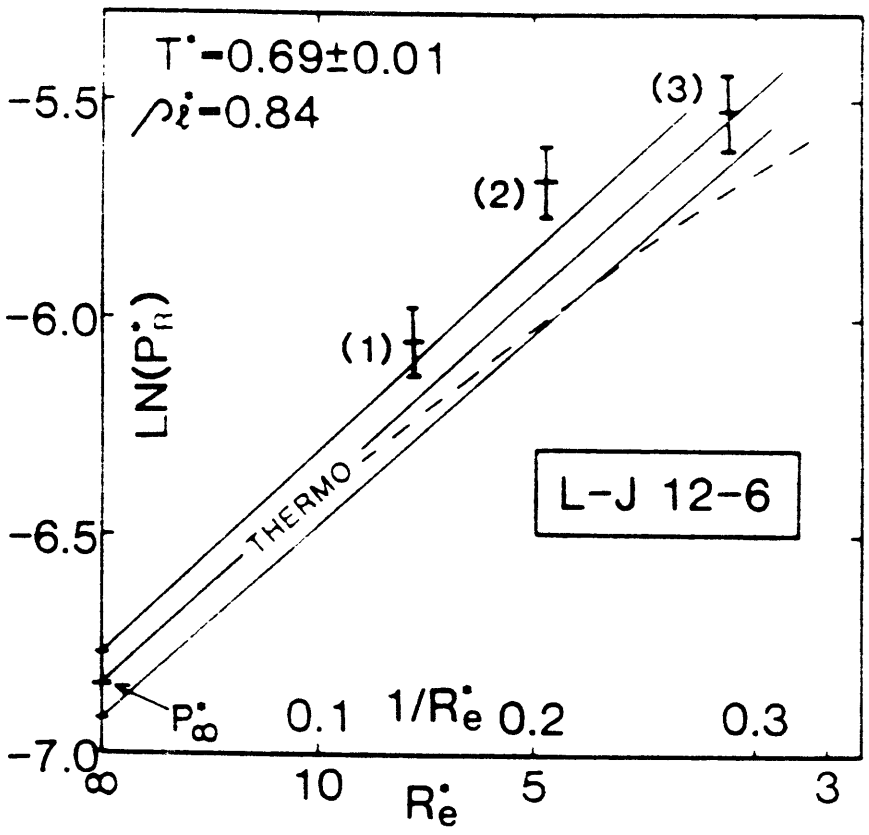

Figure 5-4: Simulation results from [24] for $T = 0.69$ and $\rho = 0.84$. The dashed line shows the introduction of a Tolman correction which results in worse agreement.

Kelvin equation makes the agreement between their simulation results and the Kelvin equation significantly worse.

Some additional uncertainty is also introduced in our calculations by the estimation of the value of γ_∞ as a function of temperature owing to its sensitivity to the cut-off radius used in simulations. We use the experimental data for the full Lennard-Jones potential in [33] which are expected to slightly overpredict the values of γ_∞, but are preferred over the simulation results in [6], for two reasons: first, our simulation cut-off is longer (and hence closer to the full Lennard-Jones potential) than the one used in the above simulations, and second, our potential is not shifted such that $V(r_c) = 0$ [6]. We estimate the combined error in our estimation of the critical radii for both evaporation and condensation to be $\pm 15\%$.

5.2.2 Heating Rate Effect

In this section we want to show that the heating rate has a negligible effect on the temperature history recovered by our simulations (Fig. 4-1). In homogeneous nucleation, phase separation proceeds when a certain number of nucleation sites of order 1 (in the statistical sense) is present. Hence, when a system enters the metastable region the history of the path taken has to be considered because of the continuous nucleation "attempts" that take place while the system is in any metastable state.

More specifically, if we denote the (given) number of nucleation sites required for nucleation $\tilde{N}$, we require that

$$\tilde{N} = \int_0^t J dt \tag{5.8}$$

where t is the time required to nucleation. We substitute for J from equation (5.1) to obtain

$$\tilde{N} = \int_{T_0}^{T} 10^{a\{1 - e^{[-(T - T_0)G/a]}\}} \frac{dT}{\dot{T}}. \tag{5.9}$$

Note that we have replaced the time integration with integration over temperature by assuming a known temperature change rate ($\dot{T}$). We will assume that ($\dot{T}$) is a constant and proportional to the heating rate $\dot{Q}$. This assumption is justified due to the very sensitive exponential term that will dominate the contribution to this integral

and make any contribution from the slowly varying ($\dot{T}$) term totally negligible. The limits of the integration are now the temperature at which nucleation will take place T, and T_0, below which nucleation rates are negligible (eq. (5.2)).

After some algebra we obtain

$$\tilde{N}\dot{T} = 10^a \int_{T_0}^{T} e^{-e^{[\ln(a\ln 10) - \frac{G}{a}(T - T_0)]}} dT \tag{5.10}$$

which after the transformation

$$y = \ln(a \ln 10) - \frac{G}{a}(T - T_0) \tag{5.11}$$

can be written as

$$\tilde{N}\dot{T} = -\frac{a}{G} 10^a \int_{\ln(a\ln 10)}^{y} e^{-e^y}\, dy. \tag{5.12}$$

By using the transformation

$$z = -e^y \tag{5.13}$$

we convert the integrand to the following integrable form:

$$\tilde{N}\dot{T} = -\frac{a}{G} 10^a \int_{-(a\ln 10)}^{z} \frac{e^z}{z}\, dz. \tag{5.14}$$

The result in terms of the variable y is finally

$$\tilde{N}\dot{T} = -\frac{a}{G} 10^a \left[y - e^y + \frac{e^{2y}}{2 \times 2!} - \frac{e^{3y}}{3 \times 3!} + ... \right]_{\ln(a\ln 10)}^{y}. \tag{5.15}$$

The above expression is evaluated at $y = \ln(a \ln 10) = 4.41$ and at y which corresponds to the nucleation temperature. This temperature is expected to be close to the homogeneous nucleation point for which $y = \tilde{y} = -4.6$. For this range of values no limiting approximation to equation (5.15) can be obtained, and hence we will proceed to show that the effect of the heating rate is negligible by examining the properties of this expression when y is close to the homogeneous nucleation point.

More specifically, let us assume that we have two heating rates $\dot{T}_1$ and $\dot{T}_2 > \dot{T}_1$. From equation (5.15) we obtain

$$\tilde{N}(\dot{T}_2 - \dot{T}_1) = -\frac{a}{G}10^a \Delta y \left[1 - e^{\tilde{y}} + \frac{e^{2\tilde{y}}}{2!} - \frac{e^{3\tilde{y}}}{3!} + ...\right] \tag{5.16}$$

where we have assumed that the change in the nucleation temperature (in $y-$coordinates) $\Delta y = y_2 - y_1$ is very small, and hence all changes in terms involving y can be linearized at $y = \tilde{y}$. This assumption leads to

$$\tilde{N}(\dot{T}_2 - \dot{T}_1) = -\frac{a}{G}10^a \Delta y \, e^{-e^{\tilde{y}}} \tag{5.17}$$

which can also be obtained by the linearization of equation (5.12) at $y = \tilde{y}$. Using the numerical values of G and a for Argon, and $\tilde{N} \sim 1$ in the above equation, we see that for the heating rates characteristic of our work ($\dot{T} \sim 10^{10} sec^{-1}$)

$$|\Delta y| \sim 10^{-14}, \tag{5.18}$$

which translates to changes in nucleation temperature of the order of $|\Delta T| \sim 10^{-12}$. We therefore conclude that the assumption of small Δy is indeed valid thus justifying the use linearization of equation (5.15) around $y = \tilde{y}$, and that the heating rate changes have a very small effect on the temperature at which nucleation occurs.

5.3 Results and Discussion

Table 5.1 shows the results for the critical size (R_c) of vapor bubble required for evaporation of liquid Argon at the various simulation pressures (P) indicated. The coexistence data were obtained from Lotfi et al. [18]. Table 5.2 gives the critical size (R_c) of liquid droplets required for condensation to occur. As can be seen from both tables, the critical sizes are in both cases very small—of the order of a few molecular diameters, as predicted by experiments with various substances including Argon [28].

The critical radii for the condensation are significantly lower than the ones found

Table 5.1: Evaporation

$P = P_l(\varepsilon/\sigma^3)$	$T_C = T_{sat}(P_v)$	$P_v(\varepsilon/\sigma^3)$	$R_c(\sigma)$
0.07	1.27	0.108	5.8
0.047	1.23	0.092	5.9
0.035	1.22	0.088	5.3

Table 5.2: Condensation

$P = P_v(\varepsilon/\sigma^3)$	$T_{sat}(P_\infty) = T_F$	$P_\infty(\varepsilon/\sigma^3)$	$R_c(\sigma)$
0.07	1.14	0.058	3.6
0.047	0.99	0.028	3.2
0.035	0.89	0.009	1.7

for evaporation, which is expected because of the higher density of the liquid drops compared to the vapor bubbles. This supports the view that generation of critical embrya is kinetically limited by the number of molecules that can spontaneously come together and form a critical nucleus with a positive rate of growth [20]. The average ratio of the critical radii $k_{R_c} \sim 1.8$ (from tables I and II) predicts a density ratio $k_\rho \propto (k_{R_c})^3 = 5.8$ which is in good agreement with the density ratio between the metastable liquid at F and metastable vapor at C ($\rho_F/\rho_C = 3.4$).

Our simulations predict critical radii for evaporation in the range $18 < R_c < 22$Å, which is in good qualitative agreement with experimental data [28] that report critical bubble radii of the order of $\sim$ 34 Å and nucleation rates of the order of $10^{30} m^{-3} s^{-1}$ for the same pressure. The latter data have been obtained under experimental conditions and thus do not necessarily represent the homogeneous nucleation limit. Indeed our simulations have achieved higher supersaturations; using the classical nucleation theory equation (5.1) and also Argon critical properties $P_c = 0.126\varepsilon/\sigma^3$, and $T_c = 1.31$, to calculate the values of constants a and G in equation (5.1), we find that for $P = 0.07\varepsilon/\sigma^3$ a nucleation temperature $\tilde{T} = 1.27$ requires a nucleation rate of

Table 5.3: Vapor and liquid spinodals

T	$\rho_{sp}(\sigma^{-3})$(Simulation)	$\rho_{sp}(\sigma^{-3})$(Theory)	Description
1.27	0.45	0.46	Liquid
1.14	0.14	0.15	Vapor
1.23	0.48	0.48	Liquid
0.99	0.12	0.12	Vapor
1.22	0.48	0.49	Liquid
0.89	0.08	0.10	Vapor

the order of $10^{36}m^{-3}s^{-1}$. Note again that the smaller critical nuclei imply higher penetration into the metastable region and higher nucleation rates. This is consistent with the size and timescales of our simulation: the volume of the simulation cell for the baseline simulation at point C is $\sim 5\times10^{-26}m^3$, and the timescale of heat addition is $\sim 10^{-10}s$. Therefore nucleation is plausible for nucleation rates that are strictly greater than $\sim 2 \times 10^{35}m^{-3}s^{-1}$ and is, therefore, possible in our simulations. Simulations with one order of magnitude more molecules (3840) would require nucleation rates greater than $\sim 2 \times 10^{34}m^{-3}s^{-1}$. We have performed such calculations and obtained identical results which indicates that the nucleation rate observed in our simulations was not a result of the limitations imposed on it through the simulation procedure.

Table 5.3 shows the comparison between theoretical results [16] for the location of the liquid and vapor spinodal on a $T-\rho$ diagram from (Fig. 5-1), and our simulation results. The second column gives the simulation result for the density as a function of the temperature and the third column gives the results of [16] at the same temperature. The spinodal branch (vapor—liquid) is indicated in the fourth column. The agreement is very good showing that we have recovered correctly the dynamics of the metastable system all the way to the spinodal.

Unfortunately, the timescales of our simulations are too short to allow a careful examination of the exact mechanism responsible for the phase domain growth. Although this is a subject of considerable interest, its simulation requires comput-

ing resources that are a few orders of magnitude away from what was available for the purposes of this study. Although our simulations are consistent with the initial homogeneous nucleation charactristics, it is conceivable that further phase domain growth is contaminated by the small simulation cell size or indeed taken over by spinodal decomposition; in particular, if the nucleation kinetics are sluggish such that significant penetration beyond the spinodal occurs with no phase change, spinodal decomposition is expected to take over as the dominant phase change process [7].

Recognizing the dynamics of phase change through molecular dynamics is an issue that remains unresolved. Although Abraham and his co-workers [16] claim to have captured the dynamics of spinodal decomposition by MD, more recent studies [11] claim that no phase separation has been observed in similar simulations. Further work is clearly required for the complete resolution of the extremely important topic of the dynamics of phase change.

Chapter 6

Summary and Future Work

We have developed a technique for simulating external heat addition in molecular dynamics simulations. The formulation requires the energy of the molecules to increase linearly in time. This is achieved by incorporating the above constraint into the equations of motion of the molecules through Gauss' principle of least constraint.

Uniformly heated fluid Argon in a two-dimensional infinite (periodic) channel was used to validate the technique. The simulation results were compared to the exact (continuum) solution and estimates for the fluid thermal conductivity were obtained. The results are in very good agreement with previous simulations using the Newtonian equations of motion and hence, the simulation method is believed to not affect the macroscopic properties of the simulated materials.

We subsequently model the constant pressure evaporation of liquid Argon in real time. The results are in good agreement with previous simulations of the equilibrium phase change properties of a Lennard-Jones model for fluid Argon. The saturation temperatures and densities as a function of the simulation pressure compare favorably with published results of both MD and Monte Carlo simulation techniques. Our results are also independent of the number of molecules in the system and the heating rate applied.

Our results are also consistent with the linear response theory interpretation of quasistatic simulations of phase change performed by other researchers: the time dependent path of the system in the two phase region contains the states accessed

by quasistatic simulations. The existence of metastable equilibrium states in the two phase region, predicted both by experimental data and theoretical considerations of nucleation theory, and more generally, the role of surface effects on phase transition, is thus verified.

Evaporation and condensation of Argon at different constant pressures is used to locate the vapor and liquid spinodal. Comparison with theoretical calculations shows very good agreement. Homogeneous nucleation theory was used to analyze the spinodal points, which represent the limiting states for which phase change takes place by nucleation and growth. Further penetration into the unstable region results in phase change by spinodal decomposition. The critical sizes for nuclei found in this work is $\sim 3\sigma$ for critical liquid drops (condensation), and $\sim 6\sigma$ for critical vapor bubbles (evaporation), consistent with experimental data and the length-scales of the simulation. The nucleation rates required for the critical radii reported above are also consistent with the simulation time-scales.

Future work should include the investigation of the growth of phase domains that was impossible in this study due to the very short time-scales of our simulation. Such work will address questions regarding the exact mechanism of phase change very close to the spinodal. Finally the effect of impurities and heterogeneous nucleation are topics of both practical and theoretical significance.

Bibliography

[1] Gas encyclopaedia, 1976.

[2] D. J. Adams. Calculating the high-temperature vapour line by Monte Carlo. *Mol. Phys.*, 37:211–221, 1979.

[3] C. J. Adkins. *Equilibrium Thermodynamics.* McGraw-Hill, 1968.

[4] M. P. Allen and D. J. Tildesley. *Computer Simulation of Liquids.* Oxford University Press, 1987.

[5] H. J. Berendsen, J. P. Postma, W. F. van Gunsteren, A. DiNola, and J. R. Haak. Molecular dynamics with coupling to an external bath. *J. Chem. Phys.*, 81:3684–3690, 1984.

[6] G. A. Chapela, G. Saville, S. M. Thompson, and J. S. Rowlinson. Computer simulation of a gas-liquid surface, part 1. *J. Chem. Soc. Faraday Trans. 2*, 73:1133–1144, 1977.

[7] P. G. Debenedetti. *Metastable Liquids. Concepts and Principles.* Princeton, 1996.

[8] D.J. Evans and G.P. Morriss. *Statistical Mechanics of Nonequilibrium Liquids.* Academic Press, 1990.

[9] J. Frenkel. *Kinetic Theory of Liquids.* Dover, New York, 1955.

[10] P. Glansdorff and I. Prigogine. *Thermodynamic Theory of Structure, Stability and Fluctuations.* Wiley-Interscience, New York, 1971.

[11] Y. Guissani and B. Guillot. A Computer simulation study of the liquid-vapor coexistence curve of water. *J. Chem. Phys.*, 98:8221–8235, 1993.

[12] J.-P. Hansen and L. Verlet. Phase transitions of the Lennard-Jones system. *Physical Review*, 184:151–161, 1969.

[13] T. L. Hill. On first-order phase transitions in canonical and grand ensembles. *J. Chem. Phys.*, 23:812–816, 1955.

[14] J. O. Hirschfelder, C. F. Curtis, and B. B. Bird. *Molecular Theory of Gases and Liquids.* Wiley, 1954.

[15] J. H. Irving and J. G Kirkwood. The statistical mechanical theory of transport processes. IV. The equations of hydrodynamics. *J. Chem. Phys.*, 17:817–829, 1950.

[16] W. E. Langlois and F. F. Abraham. On the dynamics of spinodal decomposition: A numerical solution of a generalized diffusion equation. *Chem. Phys. Lett.*, 52:129–132, 1977.

[17] J. H. Lienhard, N. Shamsundar, and P. O. Biney. Spinodal lines and equations of state: A review. *Nuclear Engineering and Design*, 95:297–314, 1986.

[18] A. Lotfi, J. Vrabec, and J. Fischer. Vapour liquid equilibria of the Lennard-Jones fluid from the NpT plus test particle method. *Mol. Phys.*, 76:1319–1333, 1992.

[19] J. E. McDonald. Homogeneous nucleation of vapor condensation I. Thermodynamic aspects. *American Journal of Physics*, 30:870–877, 1962.

[20] J. E. McDonald. Homogeneous nucleation of vapor condensation II. Kinetic aspects. *American Journal of Physics*, 31:31–41, 1963.

[21] J. J. Nicolas, K. E. Gubbins, W. B. Streett, and D. J. Tildesley. Equation of state for the Lennard-Jones fluid. *Mol. Phys.*, 37:1429–1454, 1979.

[22] M. Parinello and A. Rahman. Polymorphic transitions in single crystals: A new molecular dynamics method. *Journal of Applied Physics*, 52:7182–7190, 1981.

[23] J. G. Powles. The liquid-vapour coexistence line for Lennard-Jones-type fluids. *Physica*, 126A:289–299, 1984.

[24] J. G. Powles, R. F. Fowler, and W. A. B. Evans. A new method for computing surface tension using a drop of liquid. *Chem. Phys. Lett.*, 96:289–292, 1983.

[25] M. Rao and B. J. Berne. On the location of the surface of tension in the planar interface between liquid and vapour. *Mol. Phys*, 37:455–461, 1979.

[26] K. Refson. Molecular dynamics simulation of n-butane. *Physica*, 131:256–266, 1985.

[27] V. P. Skripov. *Metastable Liquids.* Wiley, 1974.

[28] V. P. Skripov, E. N. Sinitsyn, P. A. Pavlov, G. V. Ermakov, G. N. Muratov, N. V. Bulatov, and V. G. Baidakov. *Thermophysical Properties of Liquids in the Metastable (Superheated) State.* Gordon and Breach, 1988.

[29] A. Tenenbaum, G. Ciccotti, and R. Gallico. Stationary nonequilibrium states by molecular dynamics. Fourier's law. *Phys. Rev. A*, 25:2778–2787, 1982.

[30] P. A. Thompson and M. O. Robbins. Simulations of contact-line motion: Slip and the dynamic contact angle. *Phys. Rev. Lett.*, 63:766–769, 1989.

[31] S. M. Thompson, K. E. Gubbins, J. P. R. B. Walton, R. A. R. Chantry, and J. S. Rowlinson. A molecular dynamics study of liquid drops. *J. Chem. Phys.*, 81:527–542, 1984.

[32] R. C. Tolman. The effect of droplet size on surface tension. *J. Chem. Phys.*, 17:333–337, 1949.

[33] S. Toxvaerd. Perturbation theory for nonuniform fluids: Surface tension. *J. Chem. Phys.*, 55:3116–3120, 1971.

[34] C. Trozzi and G. Ciccotti. Stationary nonequilibrium states by molecular dynamics. II Newton's law. *Phys. Rev. A*, 29:916–925, 1984.

[35] J. P. R. B. Walton, D. J. Tildesley, and J. S. Rowlinson. The pressure tensor at the planar surface of a liquid. *Mol. Phys.*, 48:1357–1368, 1983.